

AD-A043 324

SCIENCE APPLICATIONS INC LA JOLLA CALIF
UV PHOTON AND ELECTRON DEPOSITION IN THE ATMOSPHERE.(U)
AUG 76 B F MYERS, M R SCHOONOVER

F/G 20/8

UNCLASSIFIED

SAI-76-696-LJ

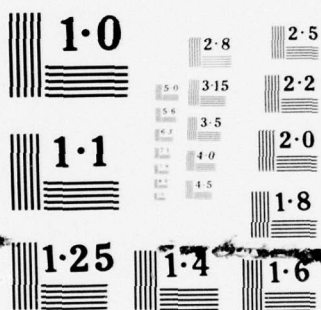
DNA-4068F

DNA001-74-C-0149

NL

1 OF 2
ADA
043324





NATIONAL BUREAU OF STANDARDS
MICROCOPY RESOLUTION TEST CHART

AD A 043324

DNA 4068F

(12)
NW

UV PHOTON AND ELECTRON DEPOSITION IN THE ATMOSPHERE

Science Applications, Inc.
P.O. Box 2351
La Jolla, California 92038

2 August 1976

Final Report for Period 7 January 1974—30 June 1976

CONTRACT No. DNA 001-74-C-0149

APPROVED FOR PUBLIC RELEASE;
DISTRIBUTION UNLIMITED.

THIS WORK SPONSORED BY THE DEFENSE NUCLEAR AGENCY
UNDER RDT&E RMSS CODE B322074462 L24AAXYX96618 H2590D.

DDC
RECEIVED
AUG 25 1977
C

AD NU.
DDC FILE COPY

Prepared for

Director
DEFENSE NUCLEAR AGENCY
Washington, D. C. 20305

Destroy this report when it is no longer
needed. Do not return to sender.



UNCLASSIFIED

SECURITY CLASSIFICATION OF THIS PAGE (When Data Entered)

REPORT DOCUMENTATION PAGE		READ INSTRUCTIONS BEFORE COMPLETING FORM
1. REPORT NUMBER DNA 4068F	2. GOVT ACCESSION NO.	3. RECIPIENT'S CATALOG NUMBER
4. TITLE (and Subtitle) UV PHOTON AND ELECTRON DEPOSITION IN THE ATMOSPHERE	5. TYPE OF REPORT & PERIOD COVERED Final Report for Period 7 Jan 74 - 30 Jun 76	
7. AUTHOR(s) Benjamin F. Myers Melvin R. Schoonover	6. PERFORMING ORG. REPORT NUMBER SAI-76-696-LJ	
9. PERFORMING ORGANIZATION NAME AND ADDRESS Science Applications, Inc. P.O. Box 2351 La Jolla, California 92038	8. CONTRACT OR GRANT NUMBER(s) DNA 001-74-C-0149	
11. CONTROLLING OFFICE NAME AND ADDRESS Director Defense Nuclear Agency Washington, D.C. 20305	10. PROGRAM ELEMENT, PROJECT, TASK AREA & WORK UNIT NUMBERS NWET Subtask L24AAXYX966-18	
14. MONITORING AGENCY NAME & ADDRESS (if different from Controlling Office)	12. REPORT DATE 2 August 1976	
	13. NUMBER OF PAGES 102	
	15. SECURITY CLASS. (of this report) UNCLASSIFIED	
	15a. DECLASSIFICATION/DOWNGRADING SCHEDULE	
16. DISTRIBUTION STATEMENT (of this Report) Approved for public release; distribution unlimited.		
17. DISTRIBUTION STATEMENT (of the abstract entered in Block 20, if different from Report)		
18. SUPPLEMENTARY NOTES This work sponsored by the Defense Nuclear Agency under RDT&E RMSS Code B322074462 L24AAXYX96618 H2590D.		
19. KEY WORDS (Continue on reverse side if necessary and identify by block number) UV Absorption Electron Absorption Atmospheric Species and Energy Densities Disturbed Atmospheres Electron Flux Spectra Predissociation of N ₂		
20. ABSTRACT (Continue on reverse side if necessary and identify by block number) The initial species, partitioning of energy, electron flux spectra and derived quantities resulting from UV photon and electron absorption by atmospheric species are calculated for the altitude range 60 to 500 km and for photon and electron energies between 10 and 300 eV and 14 and 900 eV, respectively. Cross-section curves for electron impact excitation of nitrogen to predissociating states are derived.		

DD FORM 1473

1 JAN 73

EDITION OF 1 NOV 65 IS OBSOLETE

UNCLASSIFIED

SECURITY CLASSIFICATION OF THIS PAGE (When Data Entered)

388862-72

ACCESSION for	White Section	<input checked="" type="checkbox"/>
NTIS	B. ff Section	<input type="checkbox"/>
DDC	UNANNOUNCED	<input type="checkbox"/>
JUSTIFICATION		
BY	DISTRIBUTION/AVAILABILITY	90'S
		DATE
		A

SUMMARY

The consequences of UV photon and electron deposition in the natural and disturbed atmosphere between 60 and 500 km are calculated in terms of the initial species formed, the partitioning of energy, electron flux spectra and other derived quantities. The photon energies were between 10 and 300 eV and the initial electron energies between 14 and 900 eV.

The differential electron energy slowing-down spectrum is calculated by a method which accounts for the discrete energy loss. In the calculations, reliance is placed primarily on experimental measurements as a source of input data.

In the absorption of UV photons, the initial species formed are smooth functions of the photon energy for energies above 16 eV; the total number of electrons formed per absorbed photon is relatively simply described as a function of photon energy. Most of the photon energy is required for dissociation and ionization but about 10 - 20% flows into electronic excitation while about 4 - 7% flows into vibrational excitation (at altitudes not greater than 145 km). The energy required per ion pair formed after photoabsorption is consistent with the required energy as calculated for electron deposition. In the disturbed atmosphere, represented by increases in background electron density by factors up to 10^4 (10^{12} at 60 km), positive ion densities were unaffected for photon energies less than 34 eV.

The electron deposition calculations represent an improvement on previous calculations [MS-75] by use of more accurate

cross-sections for excitation of molecular nitrogen. The principal change in the results of the calculations for the natural atmosphere is a reduction in the predicted nitrogen atom densities by 40 - 45% in the altitude range of 60 to 145 km.

Data on the electron excitation of molecular nitrogen to pre-dissociating states are reviewed and cross-section curves are derived for these states. Use of these curves in calculations of electron-N₂ interactions leads to a value of the energy required per ion-pair formed in agreement with experimental observations.

TABLE OF CONTENTS

	<u>Page</u>
1. INTRODUCTION	9
2. UV PHOTON DEPOSITION	11
2.1 Method of Calculation	11
2.1.1 High-Energy Electrons	11
2.1.2 Species and Energy Densities	13
2.1.3 Thermal Electrons	15
2.1.4 Energy Transformations	15
2.1.5 Derived Quantities	16
2.2 Processes and Data	17
2.2.1 Photoabsorption	17
2.2.2 Collisional Excitation	22
2.2.3 Radiative Decay	23
2.2.4 Conditions of the Calculations	23
2.3 Results	26
2.3.1 Initial Species	26
2.3.2 Energy Partitioning	36
2.3.3 Electron Flux Spectra	46
2.3.4 Disturbed Atmospheres	48
3. ELECTRON ENERGY DEPOSITION	53
3.1 Conditions of the Calculations	53
3.2 Results	53
3.2.1 Initial Species	55
3.2.2 Energy Partitioning	55
3.2.3 Loss Functions	61

	<u>Page</u>
3. (Continued)	
3.2.4 Electron Flux Spectra	61
3.2.5 Disturbed Atmospheres	61
4. EXCITATION TO PREDISSOCIATING STATES OF NITROGEN	65
4.1 Predissociation of Nitrogen	65
4.2 Excitation Cross-Sections	69
4.2.1 Total Cross-Section Values	71
4.2.2 Cross-Section Values for Specific States	76
4.3 Consistency and Comparison of Results	79
5. REFERENCES	81
APPENDIX A. Guide to Data Available on Microfiche	87
DISTRIBUTION LIST	99

LIST OF FIGURES

<u>Fig.</u>	<u>Title</u>	<u>Page</u>
1	Electron Volts per Ion Pair vs Photon Energy at Selected Altitudes	43
2	Comparison Between Electron Volts per Ion Pair Resulting from Deposition of Photoelectron and Incident Electron	45
3	Electron Flux Spectrum and Dependence of Flux on Photon Energy at 60 km	47
4	Photoelectron Flux Spectra from Absorption of 20.67 eV Photons at Various Altitudes	49
5	Electron Flux Spectra at 145 km for Various Background Electron Densities Following Absorption of 20.67 eV Photons	52
6	Loss Functions for N_2 , O_2 and O	62
7	Cross-Section Curve for Excitation to $N_2(a^1\Pi_g)$: Adjustment of Relative Cross-Section Data	73

LIST OF TABLES

<u>Table</u>	<u>Title</u>	<u>Page</u>
1	Species and Energy Quantities	18
2	Data on Photon Groups	19
3	Radiative Processes Regarded as Instantaneous	24
4	Input Data for Photon Deposition Calculations	25
5a	Species Densities per Absorbed Photon at 60 km and Ambient Electron Density ($[e]_{\text{amb}} = 10 \text{ cm}^{-3}$)	27
5b	Species Densities per Absorbed Photon at 110 km and Ambient Electron Density ($[e]_{\text{amb}} = 10^5 \text{ cm}^{-3}$)	28
5c	Species Densities per Absorbed Photon at 145 km and Ambient Electron Density ($[e]_{\text{amb}} = 2 \times 10^5 \text{ cm}^{-3}$)	29
5d	Species Densities per Absorbed Photon at 250 km and Ambient Electron Density ($[e]_{\text{amb}} = 6.3 \times 10^5 \text{ cm}^{-3}$)	30
5e	Species Densities per Absorbed Photon in Atomic Oxygen; Ambient Electron Density of $2.6 \times 10^5 \text{ cm}^{-3}$	31
5f	Species Densities per Absorbed Photon in Nitrogen; Ambient Electron Density of 10^5 cm^{-3}	32
5g	Species Densities per Absorbed Photon in Oxygen; Ambient Electron Density of 10^5 cm^{-3}	33
6	Constants for the Relation Between Electrons Formed per Absorbed Photon and Absorber	36
7a	Energy Partitioning for Varying Altitudes and Photon Energies	37
7b	Energy Partitioning in Single Component Gases for Varying Photon Energies	38
8	Electron Volts per Ion Pair Formed on Photon Absorption	42
9	Input Data for Electron Deposition Calculations	54

<u>Table</u>	<u>Title</u>	<u>Page</u>
10a	Species Densities per Ion Pair at 60 km and Ambient Electron Density	56
10b	Species Densities per Ion Pair at 110 km and Ambient Electron Density	56
10c	Species Densities per Ion Pair at 145 km and Ambient Electron Density	57
10d	Species Densities per Ion Pair at 250 km and Ambient Electron Density	57
10e	Species Densities per Ion Pair in Molecular Oxygen	58
10f	Species Densities per Ion Pair in Molecular Nitrogen	58
10g	Species Densities per Ion Pair in Atomic Oxygen	58
11a	Energy Partitioning for Varying Altitudes and Source Electron Flux Energies	59
11b	Energy Partitioning for Single Constituent Gases and Varying Source Electron Flux Energies	60
12	Fractional Predissociation (f_p) for Excited Electronic States of Nitrogen	70
13	Relative Values of Cross Sections for the $b' \ ^1\Sigma_u^+$, $b \ ^1\Pi_u$, $c' \ ^1\Sigma_u^+$, $c \ ^1\Pi_u$ and $o \ ^1\Pi_u$ States at High Energies and the Corresponding Oscillator Strengths	75
14	Absolute Cross-Sections for the $a \ ^1\Pi_g$ and Pre-dissociating States	77
15	Absolute Cross-Sections for the States $c' \ ^1\Sigma_u^+$, $c \ ^1\Pi_u$, $o \ ^1\Pi_u$, $b' \ ^1\Sigma_u^+$, and $b \ ^1\Pi_u$	78
A-1	Identification of Microfiche Data for ISRADU Calculations	88
A-2	Identification of Microfiche Data for ISRAD Calculations	89

1. INTRODUCTION

Calculations are reported for the species and energy densities which result from the absorption of electrons and photons in the natural and disturbed atmosphere. These calculations are performed by a method [MS-75] which accounts for the discrete energy loss undergone by electrons resulting from the initial absorption and which yields the initial species formed, the partitioning of energy, the steady-state electron flux as well as other derived quantities.

The calculations apply to the atmosphere between 60 and 500 km altitude. In the case of photon absorption, the energy of the photons lies between 10 and 300 eV. For electron absorption, the incident energy of the electrons lies between 14 and 900 eV, generally. The calculations of electron absorption represent an improved version of previous results [MS-75]. The improvement consists primarily in the use of more accurate data on nitrogen atom formation following electron impact on molecular nitrogen.

In Section 2 of this report, the deposition of a selected set of UV photons is discussed; in Section 3, electron deposition calculations are considered; in Section 4, the data on electron impact excitation of nitrogen to predissociating states are reviewed and a consistent set of cross sections is derived. Only a summary of the results of the calculations discussed in Sections 2 and 3 is presented in this report; detailed results are available on microfiche as considered in the Appendix.

2. UV PHOTON DEPOSITION

The species and energy densities which result from absorption in the earth's atmosphere of a selected set of UV photons are calculated. The calculations are performed with a code designated ISRADU.

2.1 METHOD OF CALCULATION

The method of calculation is similar to the method previously used [MS-75] for calculating electron energy degradation in the atmosphere. In this method, the differential electron energy spectrum for the electrons which are formed in interactions following absorption is calculated by a discrete energy-loss procedure. The assumption is made that a steady state for electrons, sorted into a set of energy groups, is quickly established after absorption. In the present application, the further simplifications of local energy deposition and isotropic electron fluxes are made. The densities of species formed and of energy redistributed in the establishment of the steady state for electrons are calculated with the aid of the differential electron energy spectrum.

2.1.1 High-Energy Electrons

The total set of electrons existing after photon absorption is divided into a "high-energy," slowing-down subset comprising electrons with 30 discrete energies between 1 and 10^3 eV and a "thermal" subset characterized by an electron temperature.

Electrons in the high-energy subset only lose energy in each interaction process and are placed in the thermal subset when their energy becomes less than 1 eV. Application of the steady state assumption to the subset of high-energy electrons leads to the following expression for the density of electrons in energy group j ,

$$[e_j(\text{cm}^{-3} \text{ bin}^{-1})] = P_j/L_j \quad (1)$$

where the production rate, P_j , and loss frequency, L_j , are

$$P_j = C_{j+1,j}[e_{j+1}] + \sum_S \sum_i \varphi(i) \sigma(i,S) b_p(i,j,S)[S] \\ + \sum_S \sum_{k>j} \sum_{\alpha} [e_k] v_k \sigma_{\alpha}(k,S) b_{\alpha}(k,j,S)[S] \quad (2)$$

$$L_j = C_{j,j-1} + v_j \sum_S \sum_{\alpha} [1 - b_{\alpha}(j,j,S)] \sigma_{\alpha}(j,S)[S] \quad (3)$$

The terms on the right hand side of equation (2) refer, respectively, to the rate at which electrons leave group $j+1$ and enter group j as a result of energy loss to thermal electrons with frequency $C_{j+1,j}$ and to the rates of forming electrons in group j by photoionization (subscript p) by excitation and dissociation, including dissociative excitation (subscript $\alpha = xd$) and by ionization, including dissociative ionization (subscript $\alpha = i$). Photoionization occurs by absorption of group i photons with flux $\varphi(i)$ and photoabsorption cross-section $\sigma(i,S)$ for target S to yield electrons in energy group j with probability $b_p(i,j,S)$. The excitation, dissociation and ionization of target S with cross-section $\sigma_{\alpha}(k,S)$ occurs by impact of group k electrons having speed v_k to yield electrons in energy group j with probability $b_{\alpha}(k,j,S)$.

The structure of the electron energy groups and the method for accurately describing discrete energy losses have been previously given [MS-75].

2.1.2 Species and Energy Densities

As a result of the interactions of photons and photoelectrons with the ambient atmospheric species, a loss of target species S and a gain of species S' occur according to

$$-\frac{d[S]}{dt} = \sum_i \varphi(i) \sigma(i, S)[S] + \sum_{j \geq 1} \sum_{\alpha} [e_j] v_j \sigma_{\alpha}(j, S)[S] \quad (4)$$

and

$$\begin{aligned} \frac{d[S']}{dt} = & \sum_S \sum_i \varphi(i) \sigma(i, S) b(i, S, S')[S] \\ & + \sum_S \sum_{j \geq 1} \sum_{\alpha} [e_j] v_j \sigma_{\alpha}(j, S) b_{\alpha}(j, S, S')[S] \end{aligned} \quad (5)$$

where $\sigma(i, S)$ is the photoabsorption cross-section, $b(i, S, S')$ is the probability that product S' is formed by target S absorbing a group- i photon and $b_{\alpha}(j, S, S')$ is the probability that product S' is formed by impact of an electron in energy group j on target S in the processes of excitation ($\alpha = \text{xd}$), ionization ($\alpha = \text{i}$) and electron attachment ($\alpha = \text{A}$).

The rate of increase in total electron density is

$$\begin{aligned} \frac{d[e]}{dt} = & \sum_S \sum_{j \geq 1} \left\{ \sum_i \varphi(i) \sigma(i, S) b_p(i, j, S) \right. \\ & \left. + [e_j] v_j [\sigma_i(j, S) - \sigma_A(j, S)] \right\} [S] \end{aligned} \quad (6)$$

where $[e]$, the total electron density, is the sum of the thermal electron density and the high-energy electron density, i. e. ,

$$[e] = [e_{th}] + \sum_{j \geq 1} [e_j] \quad (7)$$

and $\sigma_A(j, S)$ is the cross section for electron attachment.

The energy-density changes are monitored for seven modes: ionization, dissociation, electronic excitation, vibrational excitation, radiation, heavy-particle translation and (molecular) rotation, and electron translation. The heavy-particle translational and rotational modes are assumed to be in equilibrium. The energy transfers into the ionization (I), dissociation (D), and electronic excitation (X_e) modes are calculated from algebraic expressions such as $\sum_{S'} \epsilon (dS'/dt)$ where ϵ represents either the ionization potential of S' , the dissociation energy per atom of S' , or the excitation energy of S' , respectively, and dS'/dt is the rate of increase in S' resulting from the changes being distinguished. Changes in the remaining energy modes are given by differential equations such as

$$\begin{aligned} \frac{dM}{dt} = & \sum_S \sum_i \epsilon_M(i, S) \phi(i, t) \sigma(i, S) [S] \\ & \pm \sum_S \sum_{j \geq 1} \sum_{\alpha} [e_j] v_j e_{M\alpha}(j, S) \sigma_{\alpha}(j, S) [S] \end{aligned} \quad (8)$$

where $M(\text{eV cm}^{-3})$ denotes electron translation (E), heavy-particle translation (K), radiation (R), or vibrational excitation (X_v), and the negative sign is used only for $M = E$. In equation (8),

$$\epsilon_M(i, S) = \sum_{S'} \epsilon_M(i, S, S') b(i, S, S') (1 - \delta_{M, X_V}) \quad (9a)$$

$$\epsilon_{Mx}(j, S) = \sum_{S'} \epsilon_{Mx}(j, S, S') b_{xd}(j, S, S') \quad (9b)$$

$$\epsilon_{Mi}(j, S) = \sum_{S'} \epsilon_{Mi}(j, S, S') b_1(j, S, S') (1 - \delta_{M, X_V}), \quad (9c)$$

where $\epsilon_M(i, S, S')$, $\epsilon_{Mx}(j, S, S')$, and $\epsilon_{Mi}(j, S, S')$ are determined by examining the energy transformations in each physical process. The quantity δ_{M, X_V} is the Kronecker delta. For $M=R$, the arguments i and j are omitted.

2.1.3 Thermal Electrons

The thermal subset of electrons has contributions from energy-degraded, high-energy electrons. The rate of increase in the thermal electron density is given by equation (2) with j understood to represent the thermal subset. The treatment of the interaction of the high-energy and thermal subsets of electrons, previously developed [MH-75a], has been shown to be accurate.

2.1.4 Energy Transformations

The treatment of vibronic excitation and radiative decay resulting from electron impact are as previously described [MS-75]; for photoabsorption only electronic excitation was taken into account.

2.1.5 Derived Quantities

Several quantities, derived from the relations developed above and previously [MS-75], are of interest in connection with the absorption events. The quantities previously presented [MS-75] include the particles formed per ion pair, the electron volts per ion pair, the radiation rate, fluorescence efficiency, loss functions and the electron flux. The particles formed and electron volts per ion pair and the fluorescence efficiency are now calculated in the following manner while the remaining three quantities are calculated as before [MS-75]:

particles formed per ion pair,

$$P_{ip}(S') = \frac{(d[S'] / dt)}{\sum_S \sum_{j \geq 1} \left\{ \sum_i \varphi(i) \sigma(i, S) b_p(i, j, S) + [e_j] v_j \sigma_i(j, S) \right\} [S]} \quad (10)$$

electron volts per ion pair,

$$E_{ip} = \frac{E_p(i) \sum_S \sum_i \varphi(i) \sigma(i, S) [S]}{\sum_S \sum_{j \geq 1} \left\{ \sum_i \varphi(i) \sigma(i, S) b_p(i, j, S) + [e_j] v_j \sigma_i(j, S) \right\} [S]} \quad (11)$$

where $E_p(i)$ is the energy of the absorbed photon, and fluorescence efficiency,

$$\mathcal{F}_e = \frac{\epsilon_{R\alpha}(S') (d[S'] / dt)}{E_p(i)} \quad (12)$$

In addition, the number of particles of species S' per absorbed photon is calculated as follows:

particles per absorbed photon,

$$P_{ap}(S') = (d[S']/dt) / \sum_S \sum_i \phi(i) \sigma(i, S) [S] \quad (13)$$

2.2 PROCESSES AND DATA

Most of the processes and data used in the ISRADU code have been previously described [MS-75]; below, only additions and changes are considered. An updated list of the product species is given in Table 1. In calculating the rates of formation for these species, cross-section data were averaged over energy-group widths [MS-75] and were used in this numerical form in the calculations.

2.2.1 Photoabsorption

Photoabsorption was calculated for fourteen photon groups which span an energy range between 10 and 300 eV; these groups, the radiators of these groups, and the corresponding energies and nominal wavelengths are listed in Table 2. The photons were absorbed by O, N₂, O₂, and NO in their ground electronic and vibrational states.

Absorption by O(³P) was limited to the formation of the five atomic oxygen ions listed in Table 1. The cross sections were chosen from the mean of theoretical values [He-67b]; these lie between the experimental data [CS-65a, CS-68a]. Autoionization

Table 1. Species and Energy Quantities.

Product	Target			Energy, eV	Product	Target		Energy, eV
	O(³ P)	O ₂ (X ³ Σ _g ⁻)	NO(X ² Π)			N ₂ (X ¹ Σ _g ⁺)	NO(X ² Π)	
O(³ P)		a, xd, i*	a	2.56 [†]	N(⁴ S°)	a, i	a	4.88 [†]
O(¹ D)	xd	a, xd	a	1.96	N(² D°)	a	a	2.37
O(¹ S)	xd	a		4.17	N(² P°)		a	3.56
O(3s ⁵ S°)		xd		9.14	N(3s ⁴ P)	xd		10.33
O(3s ³ S°)	xd	a, xd		9.52	N(3s ² P)	xd		10.67
O(3p ³ P)		a		10.74	N(2p ⁴ 4P)	xd		10.93
O(3p ³ P)	xd	a		10.99	N(3p ⁴ D°)	xd		11.70
O(3d ³ D°)	xd			12.09	N(3p ⁴ P°)	xd		11.78
O(3s' ³ D°)	xd			12.54	N(3s' ² D)	xd		12.34
O(3s'' ³ P°)	xd			14.12	N(4s ² P)	xd		12.86
O(3d' ³ P°)	xd			15.40	N(3d ² D)	xd		13.02
O ⁺ (⁴ S°)	a, i	i		13.62	N ₂ (X ¹ Σ _g ⁺ , v>0)	xd		-
O ⁺ (² D°)	a, i			16.93	N ₂ (A ³ Σ _u ⁺)	a, xd		6.17
O ⁺ (² P°)	a, i			18.62	N ₂ (B ³ Π _g)	xd		7.35
O ⁺ (2s2p ⁴ 4P)	a			28.49	N ₂ (W ³ Δ _u)	xd		-
O ⁺ (2s2p ⁴ 2P)	a			39.98	N ₂ (a ¹ Π _u)	xd		8.55
O ⁻ (² P)		da*		1.08	N ₂ (C ³ Π _g)	xd		11.02
O ₂ (X ³ Σ _g ⁻ , v>0)		xd		-	N ₂ (E ³ Σ _u ⁺)	xd		11.87
O ₂ (a ¹ Δ _g)		xd		0.98	N ₂ (a' ¹ Σ _g ⁺)	xd		12.28
O ₂ (b ¹ Σ _g ⁺)		xd		1.63	N ₂ (b ¹ Π _u)**	xd		12.82
O ₂ (c ¹ Σ _u ⁻)		xd		4.05	N ₂ (c'; c; o)**	xd		13.92
O ₂ (B ³ Σ _u ⁻)		xd		6.12	N ₂ (b' ¹ Σ _u ⁺)**	xd		14.71
O ₂ (Rydberg) [#]		xd		~13.5	N ₂ (³ P)	i		14.53
O ₂ (X ² Π _g)		a, i		12.06	N ₂ ⁺ (X ² Σ _g ⁺)	a, i		15.58
O ₂ (a ⁴ Π _g)		a, i		16.10	N ₂ (A ² Π _g)	a, i		16.58
O ₂ (A ² Π _u)		a, i		16.81	N ₂ (B ² Σ _u ⁺)	a, i		18.75
O ₂ (b ⁴ Σ _u ⁻)		a, i		18.2	NO ⁺ (X ¹ Σ _g ⁺)		a	10.20
O ₂ (² Σ _g ⁻)		a		20.0				

* a ≡ photoabsorption; xd ≡ collisional excitation and dissociation; i ≡ collisional ionization; and da ≡ dissociative attachment.

[†] The energy reference for all monatomic products is the energy of O(³P) or N(⁴S°) except for these latter; for diatomic products as well as O(³P) or N(⁴S°), the energy reference is provided by O₂(X³Σ_g⁻) + N₂(X¹Σ_g⁺). Energy differences among levels of O(³P)_{0,1,2} have been neglected except in the treatment of fine-structure cooling.

[#] Excitation to Rydberg state of O₂ is considered only for the collection of such states and a representative energy is taken to be 13.5 eV.

** The representative energies of these states are determined on the basis of vibronic excitation by high-energy electron impact (see Section 4). The collection of states c_n¹Π_u, c_n¹Σ_u⁺, and o_n¹Π_u is represented by N₂(c'; c; o).

Table 2. Data on Photon Groups.

<u>Radiator</u>	<u>Energy, eV</u>	<u>Nominal Wavelength, Å</u>
NV	10.01	1240
NII	11.42	1085
NIII	12.52	990
CII	13.71	904
OII, OIII	14.84	834, 835
OIV	15.74	789
OIII	17.63	703
OIII	20.67	599
OIII	24.40	508
Mg IX	33.67	368
He II	40.80	304
-	65.44	189
-	130.41	95
Si XII	281.05	44

[He-68a] was not included. Production distribution probabilities, $b(i, S, S')$, were obtained from Henry [He-67b]. Instantaneous radiation by the $O^+(^4P)$ and $O^+(^2P)$ states was assumed.

Absorption by N_2 resulted in the products listed in Table 1. Cross sections were chosen from various sources [HT-63, SC-64, Hu-69, HC-69, Hu-72a]. Recent cross-section data [Ca-72] of generally higher resolution and for vibrationally-excited ground-electronic-state N_2 [CM-72c] were not used in the present calculations. Use of intermediate resolution data [BC-69] in the range from 700 to 785 Å would not significantly change the adopted cross-section values. For absorption of photon groups representing multiplets, the cross sections for lines of the multiplets were averaged, using line strengths [WS-66] as intensity weighting factors, to obtain multiplet cross-sections. In determining the degree of ionization, the cross-section data references given above, as well as other sources [SC-64, CO-65], were searched. Where the degree of ionization was less than unity, the formation of the products $N(^4S^\circ)$ and $N(^2D^\circ)$ was regarded as equally probable. At wavelengths above the ionization threshold, predissociation was considered; for photon groups of nominal wavelengths 990 Å, 904 Å, 835 Å, the fractional predissociation and products of predissociation were estimated to be, respectively 1.0 and $N(^4S^\circ) + N(^2D^\circ)$, 0.0, and 0.76 and $N(^2D^\circ) + N(^2D^\circ)$ on the basis of available data [CC-69, Dr-69].

The probabilities for ion products, $b(i, S, S')$, were obtained from Blake and Carver [BC-67] for wavelengths of 580 Å and greater; at smaller wavelengths, the probabilities were assumed

to be constant at the values for 580 \AA . For the ion products, only the ground vibrational level was assumed to be populated. This is a good approximation for $N_2^+(X \ ^2\Sigma_g^+)$ [BC-67] and $N_2^+(B \ ^2\Sigma_u^+)$ [JW-68] but for $N_2^+(A \ ^2\Pi_u)$, level $v' = 1$ may be significantly populated. Instantaneous radiation by $N_2^+(A \ ^2\Pi_u)$ and $N_2^+(B \ ^2\Sigma_u^+)$ was assumed.

The 11 products of absorption by $O_2(X \ ^3\Sigma_g^-)$ are listed in Table 1. Cross-section data were obtained from various sources [BC-66, CS-65a, Hu-69, Hu-72a, MW-67, SC-64, WZ-53]. Cross sections for multiplet photon groups were obtained as for N_2 . Photoionization coefficients were obtained from Matsunaga and Watanabe [MW-67]. The probabilities $b(i, S, S')$ at wavelengths between the ionization threshold and 580 \AA were taken from Blake and Carver [BC-67]; for wavelengths smaller than 580 \AA , the probabilities were assumed to be constant at the values for 580 \AA . Further, the relation

$$b\left(i, O_2(X \ ^1\Sigma_g^+), O_2^+(a \ ^4\Pi_u)\right) = 4 b\left(i, O_2(X \ ^1\Sigma_g^+), O_2^+(A \ ^2\Pi_u)\right)$$

was assumed; however, see Carlson and Judge [CJ-71a]. The photodissociation products are not well known [MW-67, BW-69, FW-69]. Below 930 \AA , estimates of Matsunaga and Watanabe [MW-67] and Beyer and Welge [BW-69] were used; at longer wavelengths, $O(^3P)$ and $O(^1D)$ were regarded as equally probable dissociation products. As in the case of N_2 , only the ground vibrational level of ions was assumed to be populated; this is not

a good assumption for oxygen, but apparently it is not serious for the results of the present calculations. Instantaneous radiation by $O_2^+(b\ ^4\Sigma_g^-)$, $O_2^+(A\ ^2\Pi_u)$, and $O_2^+(^2\Sigma_g^-)$ was assumed.

The products of absorption by NO were restricted to the list of six in Table 1. Cross-section data were taken from several sources [CC-65, SH-66a, Wa-58, WM-67]. Resolution of multiplets was not employed for these data as for N_2 and O_2 . Ionization coefficients [CC-65, WM-67] were arbitrarily set to unity below 580 Å. The product distribution was estimated on the basis of phase-space considerations.

2.2.2 Collisional Excitation

Additions to the cross-section data for excitation of $O(^3P)$ [MS-75] were made for the states $O(3d\ ^3D^\circ)$, $O(3s'\ ^3D^\circ)$, $O(3s''\ ^3P^\circ)$ and $O(3d'\ ^3P^\circ)$ [DL-71].

A revision of cross sections for excitation to the $b\ ^1\Pi_u$, $b'\ ^1\Sigma_u^+$, and $c'\ ^1\Sigma_u^+$ states and addition of data on excitation to the $c_n\ ^1\Pi_u$ and $o_n\ ^1\Pi_u$ states have been made. The source and treatment of these data are described in Section 4.

Excitation to Rydberg states of molecular oxygen has been included. These states are collectively treated; the excitation cross-section is based on experimental data [TW-72] obtained at an electron impact energy of 45 eV and on a cross-section curve shape of theoretical origin [SK-75]. From the experimental data, the residual cross-section (i. e., after accounting for specific excitations, ionization and elastic processes) has been interpreted as representing excitation to Rydberg states.

2.2.3 Radiative Decay

The changes made in accounting for radiative decay consist of additional processes in which the radiative transition is regarded as occurring instantaneously after excitation to the radiating state. These are presented in Table 3. The radiative decay attributed in Table 3 to Rydberg states of molecular oxygen and the states $b\ ^1\Pi_u$, $b'\ ^1\Sigma_u^+$, $c'\ ^1\Sigma_u^+$, $c\ ^1\Pi_u$ and $o\ ^1\Pi_u$ of molecular nitrogen is only partial as dissociation and predissociation are also accounted for in the transitions undergone by these states (see Section 4 for further discussion of these states of molecular nitrogen).

2.2.4 Conditions of the Calculations

For each of the fourteen photon groups of Table 2, the series of sixteen calculations (one calculation for each listed value of the electron density, $[e]$) indicated in Table 4 were made. The calculations span a range of atmospheric compositions corresponding to altitudes from 60 to 250 km. For each composition, the background ionization has (1) the ambient value (first listed on Table 4), and (2) values between two limits: at the lower limit, Coulomb interactions between high-energy and thermal electrons became an important contribution to energy loss by the high-energy electrons and at the upper limit, loss of high-energy electrons by dissociative recombination invalidates the steady-state approximation for the electron energy distribution as used in the present calculations. Also, an additional three calculations are made for compositions corresponding essentially to single species of N_2 , O_2 and O .

Table 3. Radiative Processes Regarded as Instantaneous.

Transition		Initiating Process*	τ , sec [†]	$\epsilon_R(S, S')$, eV
O(3s ⁵ S°)	→ O(³ P) + hν	a O(³ P)	6(-4) [‡]	9.14
O(3s ³ S°)	→ O(³ P) + hν	a O ₂ (X ³ Σ _g ⁺), a O(³ P)	2.6(-9)	9.52
O(3p ⁵ P)	→ O(3s ⁵ S°) + hν	a O ₂ (X ³ Σ _g ⁺), a O(³ P)	2.9(-8)	1.60
O(3p ³ P)	→ O(3s ³ S°) + hν	a O ₂ (X ³ Σ _g ⁺), a O(³ P)	3.6(-8)	1.47
O(3s' ³ D°)	→ O(³ P) + hν	a O(³ P)	4.3(-9)	12.54
O(3s' ² P°)	→ O(³ P) + hν	a O(³ P)	3.1(-9)	14.12
O(3d ³ D°)	→ O(³ P) + hν	a O(³ P)	2.6(-8)	12.09
O(3d' ³ P°)	→ O(³ P) + hν	a O(³ P)	1.3(-8)	15.40
O ⁺ (2s2p ⁴ 4P)	→ O ⁺ (⁴ S°) + hν	a O(³ P)	7.1(-10)	14.87
O ⁺ (2s2p ⁴ 2P)	→ O ⁺ (² D°) + hν	a O(³ P)	5.6(-10)	23.05
O ₂ (Rydberg)	→ O ₂ (X ³ Σ _g ⁻) + hν	xd O ₂ (X ³ Σ _g ⁻)	-	~13.5
O ₂ ⁺ (A ² Π _u)	→ O ₂ ⁺ (X ² Π _g) + hν	a O ₂ (X ³ Σ _g ⁻)	~6.7(-7)	4.75
O ₂ ⁺ (b ⁴ Σ _g ⁻)	→ O ₂ ⁺ (a ⁴ Π _u) + hν	a O ₂ (X ³ Σ _g ⁻)	≤1.2(-6)	2.1
O ₂ ⁺ (² Σ _g ⁻)	→ O ₂ ⁺ (A ² Π _u) + hν	a O ₂ (X ³ Σ _g ⁻)		3.19
N ₂ (b ¹ Π _u)	→ N ₂ (X ¹ Σ _g ⁺) + hν**	xd N ₂ (X ¹ Σ _g ⁺)	da	12.82
N ₂ (c' ¹ Σ _u ⁺)	→ N ₂ (X ¹ Σ _g ⁺) + hν**	xd N ₂ (X ¹ Σ _g ⁺)	da	13.92
N ₂ (c ¹ Π _u)	→ N ₂ (X ¹ Σ _g ⁺) + hν**	xd N ₂ (X ¹ Σ _g ⁺)		"
N ₂ (o ¹ Π _u)	→ N ₂ (X ¹ Σ _g ⁺) + hν**	xd N ₂ (X ¹ Σ _g ⁺)		"
N ₂ (b' ¹ Σ _u ⁺)	→ N ₂ (X ¹ Σ _g ⁺) + hν**	xd N ₂ (X ¹ Σ _g ⁺)	da	14.17
N ₂ ⁺ (A ² Π _u)	→ N ₂ ⁺ (X ² Σ _g ⁺) + hν	a N ₂ (X ¹ Σ _g ⁺)	~1.2(-5)	1.0
N ₂ ⁺ (B ² Σ _u ⁺)	→ N ₂ ⁺ (X ² Σ _g ⁺) + hν	a N ₂ (X ¹ Σ _g ⁺)	≤7. (-8)	3.17

* a ≡ photoabsorption; xd ≡ collisional excitation and dissociation; i ≡ collisional ionization.

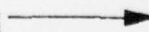
† Monatomic radiative lifetimes from WS-66; diatomic radiative lifetimes from An-71c.

‡ Decadic exponents are enclosed in parentheses.

|| da ≡ dipole allowed, CL-72.

** Only for those vibrational levels not predissociated (see Section 4).

Table 4. Input Data for Photon Deposition Calculations.

Alt, km	60	110	145	250	-	-	-
$[N_2], \text{ cm}^{-3}$	5.21(15)	1.58(12)	3.78(10)	4.35(8)	1.0(8)	5.21(15)	1.0(10)
$[O_2], \text{ cm}^{-3}$	1.40(15)	2.50(11)	4.21(9)	2.74(7)	1.0(8)	1.0(10)	1.4(15)
$[O], \text{ cm}^{-3}$	2.0(10)	3.23(11)	2.98(10)	1.91(9)	2.5(13)	1.0(10)	1.0(10)
$[NO], \text{ cm}^{-3}$	1.0(8)	5.0(7)	2.0(7)	5.0(6)	7.0(7)	7.0(7)	7.0(7)
$\theta_v, \text{ eV}$	0.0215	0.0211	0.0607	0.1105	0.122	0.0215	0.0215
$\theta, \text{ eV}$	0.0215	0.0221	0.0847	0.1656	0.218	0.0215	0.0215
$T, \text{ eV}$	0.0215	0.0211	0.0607	0.1105	0.122	0.0215	0.0215
$\varphi, \text{ cm}^{-2} \text{ sec}^{-1}$	1.0(3)	1.0(3)	1.0(3)	1.0(3)	1.0(3)	1.0(3)	1.0(3)
$[e] \text{ \& } [NO^+],$	1.0(1)	1.0(5)	2.0(5)	6.3(5)	2.6(5)	1.0(5)	1.0(5)
cm^{-3}	1.0(8)	1.0(7)	2.0(7)	6.3(7)			
	1.0(10)	1.0(9)	2.0(9)	6.3(9)			
	1.0(12)						

The densities of N_2 , O_2 and O and the neutral particle temperature (at and below 100 km) for specified altitudes were chosen from the CIRA 1972 mean atmosphere [CI-72] except for the density of O at 60 km which was based on other calculations [SL-70a]. At and below 100 km, the electron temperature was set equal to the neutral particle temperature. Above 100 km, the electron and neutral particle temperatures were based on other models [HS-75]. Densities of NO were taken from My-75. The vibrational temperature was set equal to the neutral particle temperature, and the flux value listed was arbitrarily chosen since results are normalized with respect to absorbed photons.

2.3 RESULTS

The results are presented of calculations with the ISRADU code for the depositions, in the ambient and disturbed atmosphere, of UV photons with energies in the range 10.0 to 281.05 eV and at altitudes in the range 60 to 500 km.

2.3.1 Initial Species

The initial species formed by the absorption of UV photons are listed in Table 5 in terms of the number of particles formed per absorbed photon; these quantities are calculated according to Eq. (13). The double entries for the species $N(^4S^\circ)$ and $N(^2D^\circ)$ represent the range of specific densities corresponding to the range of uncertainty associated with the predissociation of molecular nitrogen; discussion of the uncertainty in the predissociation is presented in Section 4. The initial species listed in Tables 5a through 5d correspond to photon absorption at altitudes of 60, 110, 145 and

Table 5a. Species Densities per Absorbed Photon at 60 km and Ambient Electron Density ($[e]_{\text{amb}} = 10 \text{ cm}^{-3}$).

Species	Photon Energy, eV													
	10.01	11.43	12.52	13.71	14.84	15.74	17.63	20.67	24.40	33.67	40.80	65.44	130.41	281.05
α^3P	1.00(0)	1.00(0)	6.68(-2)			3.61(-1)	6.25(-2)	3.91(-2)	1.77(-1)	2.27(-1)	2.98(-1)	4.87(-1)	8.93(-1)	1.83(0)
α^1D	1.00(0)	1.00(0)	6.68(-2)		2.90(-8)	3.31(-5)	2.71(-3)	5.04(-3)	2.22(-1)	1.03(-1)	1.71(-1)	2.85(-1)	5.17(-1)	1.04(0)
α^1S				2.75(-1)	4.09(-1)		1.26(-7)	1.92(-7)	8.66(-7)	3.72(-7)	5.63(-7)	8.64(-7)	1.62(-6)	3.50(-6)
$O^+(^4S)$				1.08(-6)	9.52(-7)	7.24(-7)	3.79(-7)	3.54(-7)	3.75(-7)	5.24(-5)	2.97(-3)	3.87(-2)	1.71(-1)	5.23(-1)
$O^+(^2D^o)$							4.63(-7)	8.66(-7)	9.12(-7)	1.17(-6)	1.73(-6)	3.03(-6)	5.33(-6)	1.01(-5)
$O_2(^1\Delta_g)$		6.07(-8)		5.62(-2)	3.92(-2)	9.83(-2)	2.57(-1)	7.90(-1)	9.89(-1)	7.27(-1)	1.05(0)	1.50(0)	2.84(0)	6.19(0)
$O_2(^1\Sigma_g^-)$		1.07(-10)		5.74(-5)	1.76(-4)	7.54(-3)	3.60(-2)	1.16(-1)	1.70(-1)	1.00(-1)	1.62(-1)	2.23(-1)	4.24(-1)	9.34(-1)
$O_2^+(X^2\Pi_g)$			1.42(-1)	1.82(-1)	1.25(-1)	2.12(-1)	2.19(-1)	2.34(-1)	2.15(-1)	2.50(-1)	3.46(-1)	4.88(-1)	8.19(-1)	1.43(0)
$O^-(^2P)$						8.90(-5)	5.99(-3)	9.36(-3)	3.37(-2)	1.09(-2)	1.54(-2)	1.52(-2)	1.56(-2)	1.61(-2)
$N(^4S^o)$	1.93(-8)	1.71(-8)	7.91(-1)			1.22(-1)	6.76(-2)		2.43(-4)	2.54(-2)	6.15(-2)	2.36(-1)	7.16(-1)	1.66(0)
$N(^4S^o)$	1.93(-8)	1.71(-8)	7.91(-1)			1.22(-1)	6.76(-2)		3.4(-4)	2.57(-2)	6.86(-2)	1.43(-1)	9.07(-1)	2.06(0)
$N(^2D^o)$	2.70(-8)	2.44(-8)	7.91(-1)		1.02(0)	1.22(-1)	6.76(-2)		2.97(-4)	3.67(-2)	9.66(-2)	3.04(-1)	8.35(-1)	1.89(0)
$N(^2D^o)$	2.70(-8)	2.44(-8)	7.91(-1)		1.02(0)	1.22(-1)	6.76(-2)		3.0(-4)	3.72(-2)	1.07(-1)	1.90(-1)	1.12(0)	2.49(0)
$N(^2P^o)$		7.33(-9)									1.84(-4)	2.19(-3)	6.39(-3)	1.42(-2)
$N_2(^3\Lambda^+\Sigma_g^-)$								4.41(-2)	5.07(-1)	1.03(0)	9.25(-1)	1.27(0)	2.20(0)	4.45(0)
$N_2(^1\Lambda^+\Pi_g)$								1.68(-3)	2.17(-2)	2.16(-1)	2.35(-1)	2.84(-1)	4.62(-1)	8.86(-1)
$N^+(^3P)$											8.64(-4)	6.88(-2)	3.52(-1)	1.04(0)
$N_2^+(X^2\Sigma_g^-)$						4.86(-1)	6.83(-1)	7.53(-1)	7.85(-1)	8.43(-1)	9.96(-1)	1.48(0)	2.53(0)	5.23(0)
$NO^+(X)$	3.40(-7)	1.46(-7)												
e	0.00	0.00	0.142	0.182	0.125	0.698	0.902	0.987	1.00	1.09	1.35	2.08	3.87	8.22

Table 5b. Species Densities per Absorbed Photon at 110 km and Ambient Electron Density ($[e]_{\text{amb}} = 10^5 \text{ cm}^{-3}$).

Species	Photon Energy, eV													
	10.01	11.43	12.52	13.71	14.84	15.74	17.63	20.67	24.40	33.67	40.80	65.44	130.41	281.05
$O(^3P)$	9.99(-1)	1.00(0)	4.31(-2)			2.42(-1)	3.78(-2)	2.17(-2)	8.51(-2)	2.08(-1)	2.57(-1)	3.97(-1)	7.17(-1)	1.45(0)
$O(^1D)$	9.99(-1)	1.00(0)	4.31(-2)		9.82(-4)	4.57(-2)	8.85(-2)	5.58(-1)	7.15(-1)	5.45(-1)	7.60(-1)	1.13(0)	2.12(0)	4.58(0)
$O(^1S)$				1.75(-1)	2.63(-1)		2.18(-3)	6.38(-3)	2.98(-2)	1.59(-2)	1.80(-2)	3.00(-2)	5.53(-2)	1.17(-1)
$O(^4S)$				6.20(-2)	5.54(-2)		2.14(-2)	1.96(-2)	2.03(-2)	5.45(-2)	7.32(-2)	1.48(-1)	3.15(-1)	6.97(-1)
$O(^2D)$							2.62(-2)	4.79(-2)	4.95(-2)	6.18(-2)	9.15(-2)	1.58(-1)	2.81(-1)	5.34(-1)
$O_2(a^1\Delta_g)$		8.12(-5)		1.71(-2)	1.59(-2)	3.55(-2)	6.90(-2)	2.76(-1)	3.66(-1)	2.78(-1)	3.55(-1)	5.43(-1)	1.02(0)	2.20(-1)
$O_2(b^1\Sigma_g^-)$		1.76(-7)		2.15(-5)	6.57(-5)	1.89(-3)	5.96(-3)	3.12(-2)	5.39(-2)	3.19(-2)	4.19(-2)	6.38(-2)	1.20(-1)	2.63(-1)
$O_2(X^2\Pi_g)$			9.15(-2)	1.16(-1)	8.06(-2)	1.42(-1)	1.37(-1)	1.43(-1)	1.29(-1)	1.47(-1)	2.05(-1)	2.82(-1)	4.78(-1)	8.34(-1)
$O(^2P)$						1.42(-5)	1.11(-3)	3.17(-3)	1.22(-2)	4.59(-3)	4.68(-3)	5.15(-3)	5.23(-3)	5.33(-3)
$N(^4S)$	5.40(-5)	4.79(-5)	8.66(-1)			1.39(-1)	7.17(-2)		1.37(-4)	2.35(-2)	5.77(-2)	2.29(-1)	7.10(-1)	1.66(0)
$N(^4S)$	5.40(-5)	4.79(-5)	8.66(-1)			1.39(-1)	7.17(-2)		1.37(-4)	2.37(-2)	6.45(-2)	2.88(-1)	9.00(-1)	2.07(0)
$N(^2D)$	7.56(-5)	6.84(-5)	8.66(-1)		1.11(0)	1.39(-1)	7.17(-2)		1.67(-4)	3.39(-2)	9.08(-2)	2.94(-1)	8.26(-1)	1.89(0)
$N(^2D)$	7.56(-5)	6.84(-5)	8.66(-1)		1.11(0)	1.39(-1)	7.17(-2)		1.67(-4)	3.42(-2)	1.01(-1)	3.83(-1)	1.11(0)	2.50(0)
$N(^2P)$		2.05(-5)									1.73(-4)	2.14(-3)	6.37(-3)	1.43(-2)
$N_2(A^3\Sigma_u^+)$								2.84(-2)	4.61(-1)	9.32(-1)	8.50(-1)	1.17(0)	2.04(0)	4.11(0)
$N_2(a^1\Pi_g)$								9.88(-4)	1.95(-2)	1.98(-1)	2.16(-1)	2.65(-1)	4.32(-1)	8.34(-1)
$N_2(X^2\Sigma_g^-)$											8.10(-4)	6.63(-2)	3.51(-1)	1.05(0)
$NO(X)$	9.50(-4)	5.47(-4)				5.54(-1)	7.25(-1)	7.82(-1)	8.01(-1)	8.45(-1)	9.95(-1)	1.46(0)	2.51(0)	5.22(0)
e	0.00	0.00	0.0915	0.178	0.136	0.740	0.010	0.993	1.00	1.11	1.37	2.12	3.94	8.34

Table 5c. Species Densities per Absorbed Photon at 145 km and
Ambient Electron Density ($[e]_{\text{amb}} = 2 \times 10^5 \text{ cm}^{-3}$).

Species	Photon Energy, eV											
	10.01	11.43	12.52	13.71	14.84	15.74	17.63	20.67	24.40	33.67	40.80	65.44
O^3P	9.78(-1)	9.87(-1)	3.16(-2)			1.63(-1)	2.42(-2)	1.26(-2)	4.74(-2)	2.95(-1)	3.66(-1)	5.37(-1)
O^1D	9.75(-1)	9.85(-1)	3.16(-2)		2.26(-3)	5.39(-2)	1.18(-1)	7.58(-1)	1.19(0)	9.30(-1)	9.97(-1)	1.66(0)
O^1S				1.10(-1)	1.69(-1)		1.77(-3)	1.11(-2)	5.26(-2)	3.67(-2)	3.26(-2)	5.88(-2)
$\text{O}^+(^4\text{S}^o)$				2.14(-1)	1.95(-1)	1.62(-1)	7.58(-2)	6.57(-2)	6.73(-2)	1.64(-1)	2.15(-1)	3.88(-1)
$\text{O}^+(^2\text{D}^o)$							9.26(-2)	1.61(-1)	1.65(-1)	1.96(-1)	2.79(-1)	4.72(-1)
$\text{O}_2(^1\Delta_g)$		6.73(-5)		3.55(-4)	6.78(-4)	3.08(-3)	6.81(-3)	3.90(-2)	7.63(-2)	5.27(-2)	5.27(-2)	9.12(-2)
$\text{O}_2(^1\Sigma_g^-)$		2.67(-6)		8.10(-6)	2.69(-5)	4.35(-4)	1.27(-3)	7.97(-3)	1.64(-2)	1.11(-2)	1.07(-2)	1.88(-2)
$\text{O}_2(^2\Pi_g)$			6.71(-2)	7.29(-2)	5.18(-2)	9.55(-2)	8.85(-2)	8.78(-2)	7.82(-2)	8.57(-2)	1.15(-1)	1.53(-1)
$\text{O}^-(^2\text{P})$						1.87(-6)	1.65(-4)	9.47(-4)	3.64(-3)	1.72(-3)	1.16(-3)	1.50(-3)
N^4S^o	1.25(-3)	1.12(-3)	9.01(-1)			1.32(-1)	6.58(-2)		6.52(-5)	1.72(-2)	4.25(-2)	1.80(-1)
N^4S^o	1.25(-3)	1.12(-3)	9.01(-1)			1.32(-1)	6.58(-2)		6.52(-5)	1.75(-2)	4.76(-2)	2.27(-1)
N^2D^o	1.75(-3)	1.60(-3)	9.01(-1)		1.02(0)	1.32(-1)	6.58(-2)		7.96(-5)	2.48(-2)	6.71(-2)	2.31(-1)
N^2D^o	1.75(-3)	1.60(-3)	9.01(-1)		1.02(0)	1.32(-1)	6.58(-2)		7.96(-5)	2.52(-2)	7.47(-2)	3.02(-1)
N^2P^o		4.80(-4)						1.64(-2)			1.30(-4)	1.69(-3)
$\text{N}_2(^3\Sigma_u^+)$									3.47(-1)	6.45(-1)	6.53(-1)	8.97(-1)
$\text{N}_2(^1\Pi_g)$									1.59(-2)	1.45(-1)	1.59(-1)	2.04(-1)
$\text{N}^+(^3\text{P})$								4.99(-4)			6.13(-4)	5.30(-2)
$\text{N}_2^+(^2\Sigma_g^+)$						5.29(-1)	6.65(-1)	6.81(-1)	6.90(-1)	7.03(-1)	7.92(-1)	1.13(0)
$\text{NO}^+(\text{X})$	2.20(-2)	1.28(-2)						0.996	1.00	1.15	1.40	2.20
e	0.022	0.013	0.0671	0.287	0.247	0.787	0.922					4.12
												8.77

Table 5d. Species Densities per Absorbed Photon at 250 km and
Ambient Electron Density ($[e]_{\text{amb}} = 6.3 \times 10^5 \text{ cm}^{-3}$).

Species	Photon Energy, eV													
	10.01	11.43	12.52	13.71	14.84	15.74	17.63	20.67	24.40	33.67	40.80	65.44	130.41	281.05
O^3P	5.58(-1)	6.77(-1)	1.86(-2)			5.54(-2)	7.91(-3)	2.89(-3)	3.91(-2)	4.58(-1)	5.63(-1)	8.78(-1)	1.66(0)	3.37(0)
O^1D	5.09(-1)	6.31(-1)	1.86(-2)		3.75(-4)	3.30(-3)	3.90(-2)	1.93(-1)	5.49(-1)	4.56(-1)	5.18(-1)	8.54(-1)	1.70(0)	3.61(0)
O^1S				3.24(-2)	5.22(-2)		1.24(-4)	5.15(-3)	2.97(-2)	3.00(-2)	3.57(-2)	5.58(-2)	1.07(-1)	2.24(-1)
O^+4S^o				6.20(-1)	5.93(-1)	5.42(-1)	2.45(-1)	1.83(-1)	1.85(-1)	3.64(-1)	4.67(-1)	8.16(-1)	1.52(0)	2.99(0)
O^+2D^o							2.99(-1)	4.45(-1)	4.53(-1)	4.87(-1)	6.26(-1)	1.02(0)	1.98(0)	4.23(0)
$\text{O}_2(a^1\Delta_g)$		1.97(-5)		4.80(-7)	4.72(-6)	4.59(-5)	1.68(-4)	1.09(-3)	3.39(-3)	2.40(-3)	2.62(-3)	4.50(-3)	9.19(-3)	1.97(-2)
$\text{O}_2(b^1\Sigma_g^+)$		3.04(-6)		3.27(-8)	4.81(-7)	7.71(-6)	3.66(-5)	2.41(-4)	7.65(-4)	5.45(-4)	5.60(-4)	9.69(-4)	2.00(-3)	4.36(-3)
$\text{O}_2^+(X^2\Pi_g)$			3.96(-2)	2.15(-2)	1.60(-2)	3.25(-2)	2.90(-2)	2.49(-2)	2.18(-2)	2.18(-2)	2.69(-2)	3.34(-2)	6.02(-2)	1.21(-1)
O^+2P							1.38(-6)	4.24(-5)	1.61(-4)	7.43(-5)	6.11(-5)	7.19(-5)	7.64(-5)	7.63(-5)
N^4S^o	2.48(-2)	2.69(-2)	9.42(-1)			7.91(-9)	3.81(-2)		6.44(-6)	5.93(-3)	1.49(-2)	7.36(-2)	2.72(-1)	6.80(-1)
N^4S^o	2.48(-2)	2.69(-2)	9.42(-1)			7.96(-2)	3.81(-2)		6.44(-6)	6.07(-3)	1.67(-2)	9.30(-2)	3.46(-1)	8.47(-1)
N^2D^o	3.48(-2)	3.84(-2)	9.42(-1)		5.55(-1)	7.96(-2)	3.81(-2)		7.88(-6)	8.56(-3)	2.35(-2)	9.42(-2)	3.13(-1)	7.62(-1)
N^2D^o	3.48(-2)	3.84(-2)	9.42(-1)		5.55(-1)	7.96(-2)	3.81(-2)		7.88(-6)	8.80(-3)	2.62(-2)	1.23(-1)	4.24(-1)	1.01(0)
N^2P^o		1.15(-2)									4.90(-5)	7.00(-4)	2.47(-3)	5.93(-3)
$\text{N}_2(A^3\Sigma_u^+)$								1.32(-3)	8.65(-2)	1.89(-1)	3.31(-1)	2.99(-1)	5.71(-1)	1.22(0)
$\text{N}_2(a^1\Pi_g)$								2.97(-5)	4.85(-3)	4.92(-2)	5.44(-2)	7.58(-2)	1.31(-1)	2.51(-1)
N^+3P											2.30(-4)	2.21(-2)	1.39(-1)	4.46(-1)
$\text{N}_2^+(X^2\Sigma_g^+)$						3.18(-1)	3.86(-1)	3.41(-1)	3.41(-1)	3.19(-1)	3.24(-1)	4.41(-1)	8.58(-1)	1.99(0)
$\text{NO}^+(X)$	4.37(-1)	3.08(-1)												
e	0.437	0.308	0.0396	0.642	0.609	0.893	0.959	0.994	1.00	1.19	1.44	2.33	4.56	9.78

Table 5e. Species Densities per Absorbed Photon in Atomic Oxygen;
Ambient Electron Density of $2.6 \times 10^5 \text{ cm}^{-3}$.

Species	Photon Energy, eV													
	10.01	11.43	12.52	13.71	14.84	15.74	17.63	20.67	24.40	33.67	40.80	65.44	130.41	221.05
O^3P	2.96(-1)	4.07(-1)	1.59(-1)			2.85(-5)	4.06(-6)	1.56(-6)	1.30(-1)	6.40(-1)	7.88(-1)	1.25(0)	2.53(0)	5.34(0)
O^1D	2.96(-1)	3.23(-1)	1.59(-1)		6.01(-6)	1.73(-5)	5.32(-1)	1.22(0)	2.34(0)	1.78(0)	2.04(1)	3.68(0)	7.74(0)	1.69(1)
O^1S				1.46(-5)	2.45(-5)		3.54(-7)	2.72(-2)	1.00(-1)	6.46(-2)	8.68(-2)	1.48(-1)	3.15(-1)	6.86(-1)
$\text{O}^+(^4\text{S}^o)$				1.00(0)	1.00(0)	1.00(0)	4.50(-1)	2.90(-1)	2.90(-1)	5.14(-1)	6.27(-1)	1.09(0)	2.15(0)	4.38(0)
$\text{O}^+(^2\text{D}^o)$							5.50(-1)	7.10(-1)	7.10(-1)	7.15(-1)	8.53(-1)	1.37(0)	2.81(0)	6.37(0)
$\text{O}_2(\text{a}^1\Delta_g)$		3.24(-4)		1.87(-9)	3.25(-5)	5.41(-4)	1.32(-4)	3.07(-4)	2.30(-4)	2.28(-4)	2.78(-4)	5.01(-4)	9.92(-4)	2.07(-3)
$\text{O}_2(\text{b}^1\Sigma_g^-)$		5.06(-5)		1.28(-10)	1.77(-10)	8.21(-5)	1.76(-5)	3.83(-5)	2.85(-5)	3.14(-5)	3.74(-5)	6.68(-5)	1.32(-4)	2.73(-4)
$\text{O}_2(\text{X}^2\Pi_g)$			3.37(-1)	9.65(-6)	7.52(-6)	1.67(-5)	1.49(-5)	1.10(-5)	9.55(-6)	8.96(-6)	1.03(-5)	1.23(-5)	2.35(-5)	5.09(-5)
$\text{O}^-(^2\text{P})$							1.27(-9)	6.33(-8)	1.67(-7)	6.96(-8)	6.15(-8)	7.58(-8)	8.12(-8)	8.02(-8)
N^4S^o	3.96(-2)	4.94(-2)	5.05(-1)			2.58(-6)	1.23(-6)		8.24(-14)	1.44(-7)	3.40(-7)	1.80(-6)	7.21(-6)	1.87(-5)
N^4S^o	3.96(-2)	4.94(-2)	5.05(-1)			2.58(-6)	1.23(-6)		8.24(-14)	1.49(-7)	3.81(-7)	2.28(-6)	9.19(-6)	2.33(-5)
N^2D^o	5.54(-2)	7.05(-2)	5.05(-1)		1.64(-5)	2.58(-6)	1.23(-6)		1.01(-13)	2.09(-7)	5.36(-7)	2.31(-5)	8.27(-6)	2.08(-5)
N^2D^o	5.54(-2)	7.05(-2)	5.05(-1)		1.64(-5)	2.58(-6)	1.23(-6)		1.01(-13)	2.16(-7)	5.97(-7)	3.02(-6)	1.12(-5)	2.79(-5)
N^2P^o		2.12(-2)												
$\text{N}_2(\text{A}^3\Sigma_u^+)$								6.57(-8)	4.53(-6)	4.81(-6)		1.16(-9)	6.56(-8)	1.63(-7)
$\text{N}_2(\text{a}^1\Pi_g)$								8.21(-13)	2.69(-7)	1.20(-6)	1.40(-6)	2.01(-6)	3.77(-6)	7.62(-6)
$\text{N}^+(^3\text{P})$											5.46(-9)	5.44(-7)	3.73(-6)	1.24(-5)
$\text{N}_2^+(\text{X}^2\Sigma_g^+)$						1.03(-5)	1.25(-5)	9.48(-6)	9.39(-6)	8.29(-6)	7.77(-6)		2.18(-5)	5.34(-5)
$\text{NO}^+(\text{X})$	6.96(-1)	5.64(-1)												
e	0.696	0.564	0.337	1.00	1.00	1.00	1.00	1.00	1.00	1.23	1.48	2.46	4.96	10.75

Table 5f. Species Densities per Absorbed Photon in Nitrogen;
Ambient Electron Density of 10^5 cm^{-3} .

Species	Photon Energy, eV													
	10.01	11.43	12.52	13.71	14.84	15.74	17.63	20.67	24.40	33.67	40.80	65.44	150.41	231.05
O^3P	9.67(-1)	9.80(-1)	6.03(-7)			4.24(-6)	5.69(-7)	5.45(-7)	3.69(-6)	3.07(-6)	4.36(-7)	6.93(-6)	1.25(-5)	2.56(-5)
O^1D	9.64(-1)	9.78(-1)	6.03(-7)		1.56(-13)	2.16(-11)	1.82(-10)	5.64(-5)	3.70(-5)	3.86(-5)	6.42(-5)	7.87(-5)	1.49(-4)	3.37(-4)
O^1S				2.88(-6)	4.36(-6)		5.72(-12)	9.91(-7)	1.57(-6)	1.01(-6)	1.63(-6)	2.21(-6)	4.19(-6)	9.41(-6)
O^+4S^a				7.92(-7)	7.10(-7)	5.95(-7)	2.52(-7)	2.35(-7)	2.37(-7)	5.69(-7)	9.14(-7)	1.92(-6)	4.19(-6)	9.30(-6)
O^+2D^a							3.08(-7)	5.75(-7)	5.81(-7)	7.38(-7)	1.15(-6)	2.02(-6)	3.58(-6)	6.48(-6)
$\text{O}_2(\text{a}^1\Delta_g)$		2.06(-5)		2.10(-9)	2.25(-9)	3.40(-9)	2.09(-4)	1.12(-3)	7.12(-4)	1.08(-3)	1.31(-3)	1.91(-3)	3.51(-3)	7.48(-3)
$\text{O}_2(\text{b}^1\Sigma_g^-)$		7.32(-11)		4.32(-15)	1.34(-14)	1.25(-12)	7.44(-10)	4.54(-6)	3.87(-6)	3.35(-6)	5.53(-6)	6.91(-6)	1.31(-5)	2.97(-5)
$\text{O}_2(\text{X}^2\Pi_g)$			1.28(-6)	1.91(-5)	1.34(-6)	2.49(-6)	2.09(-6)	2.22(-6)	1.95(-6)	2.27(-6)	3.34(-6)	4.70(-6)	8.07(-6)	1.32(-5)
O^+2P						2.31(-14)	3.72(-12)	6.22(-7)	9.52(-7)	5.33(-7)	7.11(-7)	6.21(-7)	6.47(-7)	6.90(-7)
N^4S^a	1.82(-3)	1.64(-3)	1.00(0)			2.00(-1)	9.00(-2)		2.45(-9)	3.00(-2)	7.55(-2)	2.90(-1)	8.79(-1)	2.06(0)
N^4S^a	1.82(-3)	1.64(-3)	1.00(0)			2.00(-1)	9.00(-2)		2.45(-9)	3.01(-2)	8.46(-2)	3.66(-1)	1.12(0)	2.56(0)
N^2D^a	2.55(-3)	2.34(-3)	1.00(0)		1.52(0)	2.00(-1)	9.00(-2)		3.00(-9)	4.31(-2)	1.19(-1)	3.74(-1)	1.02(0)	2.33(0)
N^2D^a	2.55(-3)	2.34(-3)	1.00(0)		1.52(0)	2.00(-1)	9.00(-2)		3.00(-9)	4.32(-2)	1.33(-1)	4.87(-1)	1.38(0)	3.09(0)
N^2P^a		7.02(-4)									2.14(-4)	2.73(-3)	7.91(-3)	1.77(-2)
$\text{N}_2(\text{A}^3\Sigma_u^+)$								7.36(-7)	8.20(-1)	1.20(0)		1.51(0)	2.57(0)	5.11(0)
$\text{N}_2(\text{a}^1\Pi_g)$								1.76(-8)	1.96(-2)	2.54(-1)	2.72(-1)	3.27(-1)	5.17(-1)	9.66(-1)
N^+3P											1.00(-3)	8.50(-2)	4.34(-1)	1.30(0)
$\text{N}_2(\text{X}^2\Sigma_g^-)$						8.00(-1)	9.10(-1)	1.00(0)	1.00(0)	1.07(0)	1.34(0)	1.97(0)	3.33(0)	6.66(0)
$\text{NO}^+(\text{X})$	3.21(-2)	1.87(-2)												
e	0.0321	0.0187	1.28(-6)	2.70(-6)	2.05(-6)	0.800	0.910	1.00	1.00	1.07	1.34	2.06	3.76	7.96

Table 5g. Species Densities per Absorbed Photon in Oxygen;
Ambient Electron Density of 10^5 cm^{-3} .

Species	Photon Energy, eV													
	10.01	11.43	12.52	13.71	14.84	15.74	17.53	20.67	24.40	33.67	40.80	65.44	130.41	281.05
O^3P	1.00(0)	1.00(0)	3.20(-1)			9.20(-1)	2.52(-1)	4.04(-1)	8.11(-1)	1.95(0)	2.26(0)	3.51(0)	6.84(0)	1.44(1)
O^1D	1.00(0)	1.00(0)	3.20(-1)		7.26(-6)	1.31(-4)	1.23(-2)	2.45(-2)	1.33(-1)	7.13(-1)	1.04(0)	1.71(0)	3.25(0)	6.60(0)
O^1S				8.60(-1)	1.24(0)		2.83(-7)	2.74(-7)	8.42(-7)	1.00(-6)	1.08(-6)	1.60(-6)	3.10(-6)	6.61(-6)
O^4S^o				1.69(-6)	1.44(-6)	9.23(-7)	7.00(-7)	7.18(-7)	9.21(-7)	9.71(-4)	1.55(-2)	2.03(-1)	8.97(-1)	2.63(0)
O^2D^o							9.29(-7)	1.76(-6)	2.12(-6)	2.76(-6)	3.60(-6)	6.54(-6)	1.20(-5)	2.42(-5)
$\text{O}_2(^1\Delta_g)$		1.59(-7)		4.74(-1)	6.16(-1)	1.24(0)	1.90(0)	1.97(0)	3.04(0)	3.02(0)	3.50(0)	5.45(0)	1.03(1)	2.31(1)
$\text{O}_2(^1\Sigma_g^+)$		2.16(-8)		3.56(-2)	9.81(-2)	2.20(-1)	3.37(-1)	3.58(-1)	5.99(-1)	5.86(-1)	6.73(-1)	1.04(0)	2.06(0)	4.43(0)
$\text{O}_2(^2\Pi_g)$			6.80(-1)	5.70(-1)	3.80(-1)	5.40(-1)	8.60(-1)	9.50(-1)	1.01(0)	1.19(0)	1.39(0)	2.03(0)	3.51(0)	6.86(0)
O^2P						4.08(-4)	2.79(-2)	1.48(-2)	5.07(-2)	3.69(-2)	3.64(-2)	3.42(-2)	3.42(-2)	3.38(-2)
N^4S^o	1.35(-8)	1.20(-8)	7.27(-6)			5.95(-7)	5.21(-7)		2.18(-8)	3.26(-7)	6.61(-7)	2.45(-6)	7.43(-6)	1.66(-5)
N^4S^o	1.35(-8)	1.20(-8)	7.27(-6)			5.95(-7)	5.21(-7)		2.18(-8)	3.37(-7)	7.26(-7)	3.07(-6)	9.37(-6)	2.05(-5)
N^2D^o	1.89(-8)	1.71(-8)	7.27(-6)		5.93(-6)	5.95(-7)	5.21(-7)		2.67(-8)	4.68(-7)	1.01(-6)	3.16(-6)	8.71(-6)	1.92(-5)
N^2D^o	1.89(-8)	1.71(-8)	7.27(-6)		5.93(-6)	5.95(-7)	5.21(-7)		2.67(-8)	4.85(-7)	1.11(-6)	4.08(-6)	1.16(-5)	2.49(-5)
N^2P^o		5.13(-9)												
$\text{N}_2(\text{A}^3\Sigma_u^+)$								3.49(-6)	9.04(-6)	1.98(-5)	1.90(-5)	2.69(-5)	5.24(-5)	1.13(-4)
$\text{N}_2(\text{a}^1\Pi_g)$								1.43(-7)	8.03(-7)	3.46(-6)	3.65(-5)	4.61(-6)	8.52(-6)	1.76(-5)
$\text{N}^o(\text{P})$											9.24(-9)	6.90(-7)	3.55(-6)	1.01(-5)
$\text{N}_2^+(\text{X}^2\Sigma_g^+)$						2.38(-6)	5.27(-6)	5.87(-6)	7.02(-6)	7.54(-6)	7.69(-6)	1.24(-5)	2.28(-5)	4.89(-5)
$\text{NO}^+(\text{X})$	2.38(-7)	1.37(-7)												
e	2.38(-7)	1.37(-7)	0.690	0.570	0.380	0.540	0.880	0.950	1.01	1.19	1.41	2.24	4.41	9.49

250 km respectively; those listed in Tables 5e through 5g correspond to photon absorption in single component gases of atomic oxygen and molecular nitrogen and oxygen, respectively, with background electron densities. In the atomic oxygen case, Table 5e, the initial species also represent, to within a negligible error, those species formed at 500 km by photon absorption since the electron density used has the ambient value and the density of atomic oxygen represents about 99% of the total density at 500 km.

The species densities per absorbed photon at a fixed altitude have erratic values as a function of photon energy for energies below 16 eV. For photon energies in the range between 20 and 281 eV, the species per absorbed photon have smoothly increasing values as a function of photon energy. At the low energy end of the latter range of photon energies, neutral and ionic species are formed in comparable amounts; at the high-energy end of this range, about twice as many neutral as ionic species are formed except for a range of altitudes centered about 250 km where the respective amounts are again comparable. There is, as expected on the basis of the change in atmospheric composition with altitude, a monotonic variation of species per absorbed photon at a fixed photon energy, for many of the species.

The total number of electrons formed per absorbed photon can be represented, relatively simply, as a function of photon energy and atmospheric composition for photon energies of 15.74 eV and larger and for compositions corresponding to the range of altitudes between 60 and 500 km. On the basis of the data of the Tables 4 and 5, the total number of electrons per absorbed photon is given by

$$[e]_{ap} = 1 - 1.864 \cdot 10^4 (1 - 0.9936f_O - 1.016f_{N_2}) e^{-0.7323(1 - 0.3509f_O - 0.2319f_{N_2})E_p} \quad (14)$$

for $15.74 \leq E_p \text{ (eV)} < 28.0$ and by

$$[e]_{ap} = 1.0 + (0.05371 - 0.01519f_O - 0.03179f_{N_2})(E_p - 28.0) \quad (15)$$

for $E_p \geq 28.0$ eV. The quantities f_O and f_{N_2} are the fractional densities of O and N_2 . Equation (14) is accurate to within 3% except at 500 km for energies between 15.74 and 17.6 eV where the error can be as large as 7%; Eq. (15) is accurate to within 3%. The fact that the fractional contributions of O and N_2 to Eqs. (14) and (15) occur as first powers is a consequence of the coupling among contributions of O, N_2 and O_2 . To account for the individual contributions of these latter species to the electrons per absorbed photon requires, at least at the higher photon energies, relationships of the form

$$[e]_{ap,i} = af_i^\alpha + bf_i^\beta (E_p - E_p^\circ) \quad (16)$$

where $[e]_{ap,i}$ is the number of electrons formed per photon absorbed by species i , a , b , α , β and E_p° are constants with $\alpha, \beta \neq 1$. For the data of Tables 4 and 5, the value of these constants are given in Table 6 for photon energies greater than 33.67 eV. The sum $\sum_i [e]_{ap,i} \equiv [e]_{ap}$ gives values accurate to about 3% except for the smallest energies at the lowest altitudes (~ 60 km) and energies above 41 eV at 500 km where the errors are as large

Table 6: Constants For The Relation Between Electrons
Formed per Absorbed Photon and Absorber

Absorber	a	b	α	β	E_p°
N ₂	1.06	0.0266	0.872	0.649	33.67
O ₂	1.26	0.0238	0.927	0.821	33.67
O	1.20	0.0350	1.09	1.30	33.67

as 8%. Also note that $[e]_{ap,i} = [i^+]_{ap}$ where $[i^+]_{ap}$ is the density of ions formed from absorber i per absorbed photon and for the molecular absorbers, i^+ represents the sum of the corresponding singly charged molecular and atomic ions. To represent the electrons and ions per absorbed photon from absorber i as a function of photon energy and atmospheric composition will be more involved, for photon energies between 15.74 and 33.67 eV, than the above treatment; no attempt to obtain this representation has been made. From Table 5, it is apparent that neutral species can also be represented as a function of photon energy and atmospheric composition in a manner analogous to that for electrons and ions; again, no attempt has been made to do so.

2.3.2 Energy Partitioning

The partitioning of energy into seven modes for absorption is shown in Table 7; the values listed in the table are the fractions of the total energy appearing in mode M computed from the ratio $(dM/dt)/\sum_M (dM/dt)$ where dM/dt is calculated according to Eq. (8). The energy modes M are: heavy particle translation (K), electron translation (E), radiation (R), vibrational excitation (X_v), ionization (I),

Table 7a. Energy Partitioning for Varying Altitudes and Photon Energies.

Alt., km		Photon Energy, eV													
		10.01	11.43	12.52	13.71	14.84	15.74	17.63	20.67	24.40	33.67	40.80	65.44	130.41	281.05
50	f_M														
	f_K	0.29	0.381	0.054	0.003	0.031	0.150	0.033	0.010	0.007	0.006	0.008	0.022	0.039	0.048
	f_E			0.005	0.008	0.005	0.013	0.037	0.029	0.024	0.020	0.011	0.001	0.008	0.015
	f_R				0.596	0.161		0.049	0.056	0.069	0.155	0.172	0.180	0.179	0.168
	f_{X^v}				0.070	0.015	0.034	0.029	0.107	0.070	0.067	0.074	0.066	0.063	0.063
	f_I			0.137	0.160	0.102	0.644	0.754	0.705	0.608	0.479	0.484	0.467	0.435	0.431
	f_D	0.51	0.448	0.644	0.051	0.406	0.134	0.047	0.006	0.022	0.035	0.050	0.084	0.112	0.120
110	f_{X^e}	0.20	0.171	0.160	0.172	0.280	0.025	0.051	0.087	0.200	0.238	0.201	0.180	0.164	0.155
	f_K	0.29	0.380	0.457	0.002	0.025	0.113	0.033	0.006	0.003	0.003	0.005	0.017	0.033	0.041
	f_E			0.003	0.009	0.009	0.017	0.044	0.046	0.037	0.032	0.024	0.013	0.019	0.026
	f_R				0.643	0.176		0.044	0.049	0.063	0.168	0.185	0.190	0.187	0.177
	f_{X^v}				0.004	0.009	0.019	0.019	0.074	0.056	0.051	0.056	0.052	0.049	0.049
	f_I			0.088	0.163	0.116	0.696	0.771	0.717	0.614	0.491	0.495	0.477	0.445	0.439
	f_D	0.51	0.448	0.692	0.033	0.411	0.125	0.045	0.003	0.010	0.022	0.035	0.067	0.097	0.106
145	f_{X^e}	0.20	0.172	0.170	0.146	0.254	0.030	0.044	0.105	0.217	0.233	0.200	0.184	0.170	0.162
	f_K	0.285	0.375	0.042	0.001	0.020	0.085	0.030	0.004	0.001	0.002	0.003	0.012	0.025	0.033
	f_E		0.002	0.003	0.009	0.020	0.029	0.053	0.073	0.061	0.050	0.042	0.031	0.035	0.042
	f_R				0.576	0.161		0.037	0.039	0.054	0.189	0.206	0.205	0.199	0.185
	f_{X^v}				0.001	0.004	0.013	0.012	0.046	0.040	0.036	0.038	0.036	0.034	0.035
	f_I	0.020	0.010	0.065	0.277	0.221	0.737	0.778	0.714	0.609	0.501	0.501	0.487	0.460	0.455
	f_D	0.503	0.444	0.716	0.021	0.363	0.108	0.040	0.002	0.004	0.013	0.022	0.048	0.076	0.085
250	f_{X^e}	0.191	0.169	0.174	0.115	0.211	0.028	0.050	0.122	0.231	0.209	0.188	0.181	0.170	0.164
	f_K	0.146	0.239	0.038	0.001	0.009	0.037	0.017	0.001	0.001	0.001	0.001	0.005	0.011	0.015
	f_E	0.031	0.054	0.002	0.007	0.052	0.081	0.090	0.178	0.226	0.150	0.133	0.128	0.131	0.137
	f_R				0.299	0.088		0.020	0.018	0.035	0.215	0.230	0.220	0.207	0.191
	f_{X^v}						0.002	0.002	0.006	0.008	0.003	0.008	0.008	0.008	0.008
	f_I	0.370	0.235	0.038	0.635	0.557	0.809	0.780	0.689	0.584	0.500	0.496	0.499	0.489	0.488
	f_D	0.356	0.360	0.742	0.006	0.191	0.058	0.022	0.003	0.003	0.003	0.006	0.018	0.033	0.039
	f_{X^e}	0.097	0.112	0.180	0.052	0.103	0.123	0.069	0.108	0.146	0.123	0.126	0.122	0.121	0.122

Table 7b. Energy Partitioning in Single Component Gases for Varying Photon Energies.

Species	f_N	Photon Energy, eV														130.41	281.05
		10.01	11.43	12.52	13.71	14.84	15.74	17.63	20.67	24.40	33.67	40.80	65.44				
O	f_K	0.07	0.132	0.086					0.084	0.064	0.055	0.045	0.037	0.037	0.042		
	f_E	0.045	0.094	0.011	0.007	0.082	0.132	0.065		0.058	0.252	0.272	0.250	0.235	0.221		
	f_R						0.003			0.001							
	f_{X_v}		0.001				0.865	0.773	0.659	0.558	0.497	0.494	0.512	0.518	0.521		
	f_I	0.562	0.411	0.325	0.993	0.918											
	f_D	0.275	0.293	0.458													
	f_{X_e}	0.048	0.069	0.120				0.162	0.257	0.319	0.196	0.189	0.201	0.210	0.216		
N ₂	f_K	0.281	0.371	0.031		0.017	0.046	0.039				0.002	0.015	0.031	0.039		
	f_E	0.002	0.002				0.008	0.044	0.053	0.034	0.036	0.027	0.016	0.024	0.031		
	f_R				0.875	0.240		0.041	0.046	0.059	0.161	0.177	0.187	0.187	0.179		
	f_{X_v}		0.002					0.010	0.147	0.061	0.073	0.090	0.074	0.070	0.071		
	f_I	0.030	0.015				0.792	0.804	0.754	0.639	0.497	0.511	0.487	0.446	0.436		
	f_D	0.499	0.442	0.780		0.500	0.124	0.050			0.011	0.025	0.063	0.099	0.110		
	f_{X_e}	0.188	0.168	0.189	0.125	0.243	0.030	0.012		0.207	0.223	0.168	0.158	0.143	0.134		
O ₂	f_K	0.293	0.381	0.139	0.008	0.058	0.310	0.015	0.047	0.024	0.043	0.045	0.059	0.079	0.091		
	f_E			0.025	0.028	0.017	0.022	0.031	0.029	0.024	0.010						
	f_R							0.073	0.077	0.089	0.095	0.111	0.118	0.108	0.093		
	f_{X_v}					0.003	0.004	0.005	0.005	0.004	0.003	0.003	0.003	0.003	0.003		
	f_I			0.655	0.501	0.309	0.414	0.602	0.554	0.500	0.425	0.416	0.416	0.418	0.422		
	f_D	0.511	0.448	0.131	0.161	0.213	0.150	0.040	0.054	0.101	0.204	0.210	0.213	0.217	0.216		
	f_{X_e}	0.196	0.171	0.050	0.300	0.400	0.100	0.234	0.234	0.258	0.220	0.215	0.201	0.186	0.175		

dissociation (D), and electronic excitation (X_e). Table 7a contains data on energy partitioning for various photon energies as a function of altitude in the range between 60 and 250 km; Table 7b has data on single component gases. As before (see Section 2.3.1), the data on atomic oxygen, of Table 7b, may be regarded as the 500 km altitude calculations and thus can be used as an extension of Table 7a.

The most important energy mode at low photon energies is dissociation and at higher photon energies, ionization. A significant fraction of the energy is used in dissociating molecules following absorption of photons with energies (E_p) of 14.84 eV or less, excepting 13.71 eV; the fraction is erratic in magnitude with variation in E_p and has values as large as 0.74. This fraction declines in magnitude with increasing altitude except for $E_p = 12.52$ eV where a maximum occurs at 250 km. For $E_p > 15.75$ eV, the energy in dissociation is generally less than 0.05 up to 40.8 eV and less than 0.12 for all photon energies above 15.74 eV. At $E_p \geq 15.74$ eV, the energy in dissociation declines with altitude and, as a function of E_p , exhibits a minimum at about 20 eV. The energy in ionization is generally less than that in dissociation for $E_p \leq 14.84$ eV except at the highest altitudes. But for $E_p \geq 15.74$ eV, the fraction of energy in ionization is largest; for the altitude range from 60 to 500 km, the fraction is between 0.65 and 0.80 for photon energies in the range from 15.74 to 20.67 eV and is between 0.43 and 0.52 for $E_p \geq 33.67$ eV.

Of secondary magnitude, are the fractions of the energy in the radiation and electronic excitation modes. For $E_p \leq 14.84$ eV, the fraction of energy in the radiation mode is significant only for $E_p = 13.71$ and 14.84 eV. The large fraction in the radiation mode for $E_p = 13.71$ eV, ~ 0.6 for altitudes from 60 to 145 km, is mainly from

radiative decay of the $c' \ ^1\Sigma_u^+$ state of nitrogen (see Section 4); for photon energies of 12.52 and 14.84 eV, the nitrogen excited to the singlet valence and Rydberg states predominantly decays by predissociation. The fraction of energy in the radiation mode for energies in the range 15.74 to 24.40 eV is less than about 0.05 and generally declines with increasing altitude. For $E_p \geq 33.67$ eV, the fraction in radiation is between about 0.15 and 0.25 and increases with increasing altitude. For electronic excitation, the fraction of energy is between 0.15 and 0.25 for $E_p \leq 14.84$ eV and for altitudes in the range 60 to 145 km; the fraction declines with increasing altitude and is erratic as a function of photon energy. For $E_p \geq 15.74$ eV, the fraction of energy in electronic excitation, as a function of E_p , rises to near 30 eV and declines with further increase in E_p . The maxima are fractions in the range 0.15 to 0.30 and the declines in the fractional values at larger E_p are modest.

The fractions of energy in the electron and heavy particle translation modes and in the vibrational excitation mode are generally the smallest. The fraction in electron translation is less than about 0.15 except at 250 km for $E_p = 20.67$ and 24.40 eV. The fraction in electron translation increases with altitude except for $E_p \geq 17.63$ eV where a decline occurs between 250 and 500 km. For the heavy-particle translation, the fraction is generally in the range 0.03 to 0.05 except at $E_p = 15.74$ eV and for $E_p = 10.01$ and 11.43 eV; in the latter case, fractions are in the range 0.29 to 0.38 at low altitudes. The fraction of energy in the heavy-particle translation mode declines with increasing altitude. The fraction of energy in vibrational excitation decreases with increasing altitude, rises with E_p increasing to 20.67 eV and is relatively constant for larger E_p .

The electron volts per ion pair (E_{ip}) formed by photon absorption are listed in Table 8 and shown in Figure 1 as a function of photon energy and altitude. The listed quantities were calculated according to Eq. (11). For photon energies between 17 and 34 eV, the values of E_{ip} increase with increasing photon energy and for energies greater than 34 eV, E_{ip} moderately increases or decreases and ultimately changes only slightly with increasing photon energy. For photon energies below 17 eV, E_{ip} increases in an irregular manner with decreasing photon energy. The dependence of E_{ip} [$\equiv E_{ip}(pa)$] in photoabsorption is in contrast to the case of E_{ip} [$\equiv E_{ip}(e)$] in electron deposition [MS-75]; in the latter, well-known case, $E_{ip}(e)$ decreases monotonically with increasing (electron) energy. The differences are understood by considering the equations for $E_{ip}(pa)$ and $E_{ip}(e)$. When in the photoabsorption case, photoionization predominates, Eq. (11) may be rearranged to yield

$$E_{ip}(pa) \approx \frac{E_p(i)}{1 + \sigma(pa)} \quad (17)$$

where one represents the primary photoelectron and $\sigma(pa)$ the number of subsequently derived electrons. Between $E_p(i)$ values of 17 and 34 eV, $\sigma(pa)$ is small compared to one and $E_{ip}(pa) \approx E_p(i)$; above 34 eV, $\sigma(pa)$ is significant and as $\sigma(pa)$ increases with increasing $E_p(i)$, a moderate or slight change in $E_{ip}(pa)$ with increasing photon energy is understandable. Below 17 eV, where photon absorption to yield neutral states is important, less than one primary photoelectron is obtained on the average for absorption of energy $E_p(i)$; thus the one in the denominator of Eq. (17) is replaced by a number less than one yielding a larger value of $E_{ip}(pa)$ below 17 eV. The neutral states formed by photoabsorption below 17 eV are primarily those of N_2 . These states

Table 8. Electron Volts per Ion Pair Formed on Photon Absorption.

Alt. (km)	Photon Energy (eV)													
	10.01	11.43	12.52	13.71	14.84	15.74	17.63	20.67	24.40	33.67	40.80	65.44	130.41	281.05
60	2.95(7)	5.85(7)	88.2	75.3	118.	22.6	19.5	20.9	24.4	30.8	30.3	31.5	33.7	34.2
110	1.05(4)	2.09(4)	136.	77.1	109.	21.3	19.4	20.8	24.4	30.4	29.9	31.0	33.2	33.7
145	454.	893.	187.	47.8	60.1	20.0	19.1	20.8	24.4	29.3	29.1	29.8	31.6	32.1
250	22.9	37.1	316.	21.4	24.4	17.6	18.4	20.7	24.4	28.3	28.3	28.0	28.6	28.8
500	14.4	20.3	37.2	13.7	14.8	15.7	17.6	20.7	24.4	27.4	27.6	26.6	26.3	26.2

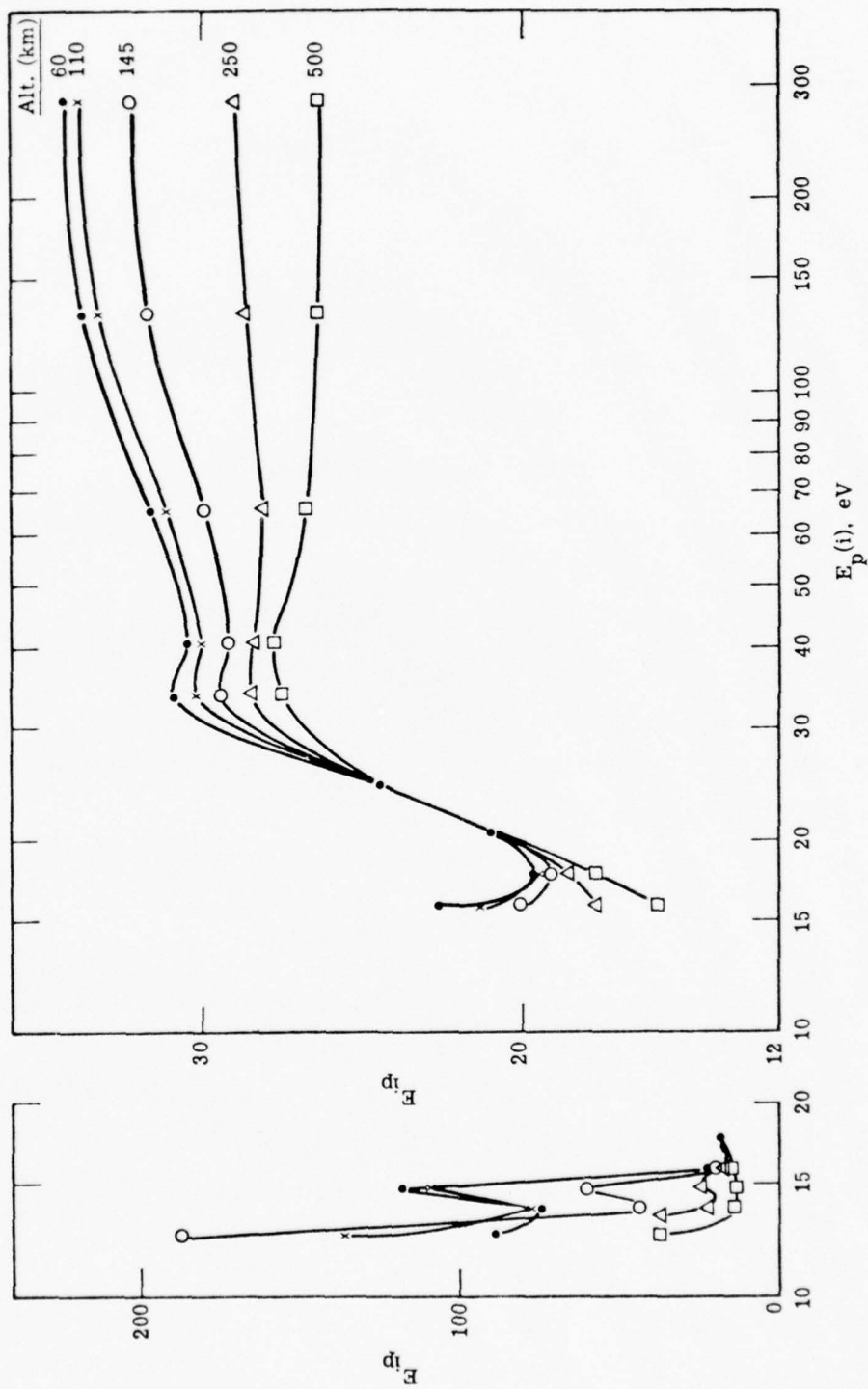


Figure 1. Electron Volts per Ion Pair vs Photon Energy at Selected Altitudes.

either predissociate, as is evident from Table 5 or radiatively decay to the ground state.

In the corresponding case of electron deposition,

$$E_{ip}(e) = \frac{\epsilon_E}{\sigma(e)} \quad (18)$$

where ϵ_E is the energy of the incident electron and $\sigma(e)$ is the number of subsequently derived electrons (i.e., primary, secondary, etc.). As ϵ_E increases, $\sigma(e)$ increases rapidly at low electron energies and in approximate proportion to ϵ_E at high energies.

The relation between Eqs. (17) and (18) is demonstrated by considering the effect of the primary photoelectron on the subsequent formation of ion pairs. The energy of the photoelectron is $E_p(i) - \bar{E}_I$ where \bar{E}_I is the average ionization energy of the target gas for the photon. Consequently, for the photoelectron with energy in excess of the smallest ionization energy of the target gas, the electron volts per ion pair, $E_{ip}(pe)$, is

$$E_{ip}(pe) = \frac{E_p(i) - \bar{E}_I}{\sigma(pa)} \quad (19)$$

This equation gives the same results as Eq. (18); this is demonstrated in Figure 2 by applying Eq. (19) to the data on Tables 4 and 5a for 60 km and comparing these results with values of $E_{ip}(e)$ taken from Table 10 in Section 3 below where the deposition of incident electrons is treated (note that $\sigma(pa) = [e] - 1$ where $[e]$ is given in Table 5a).

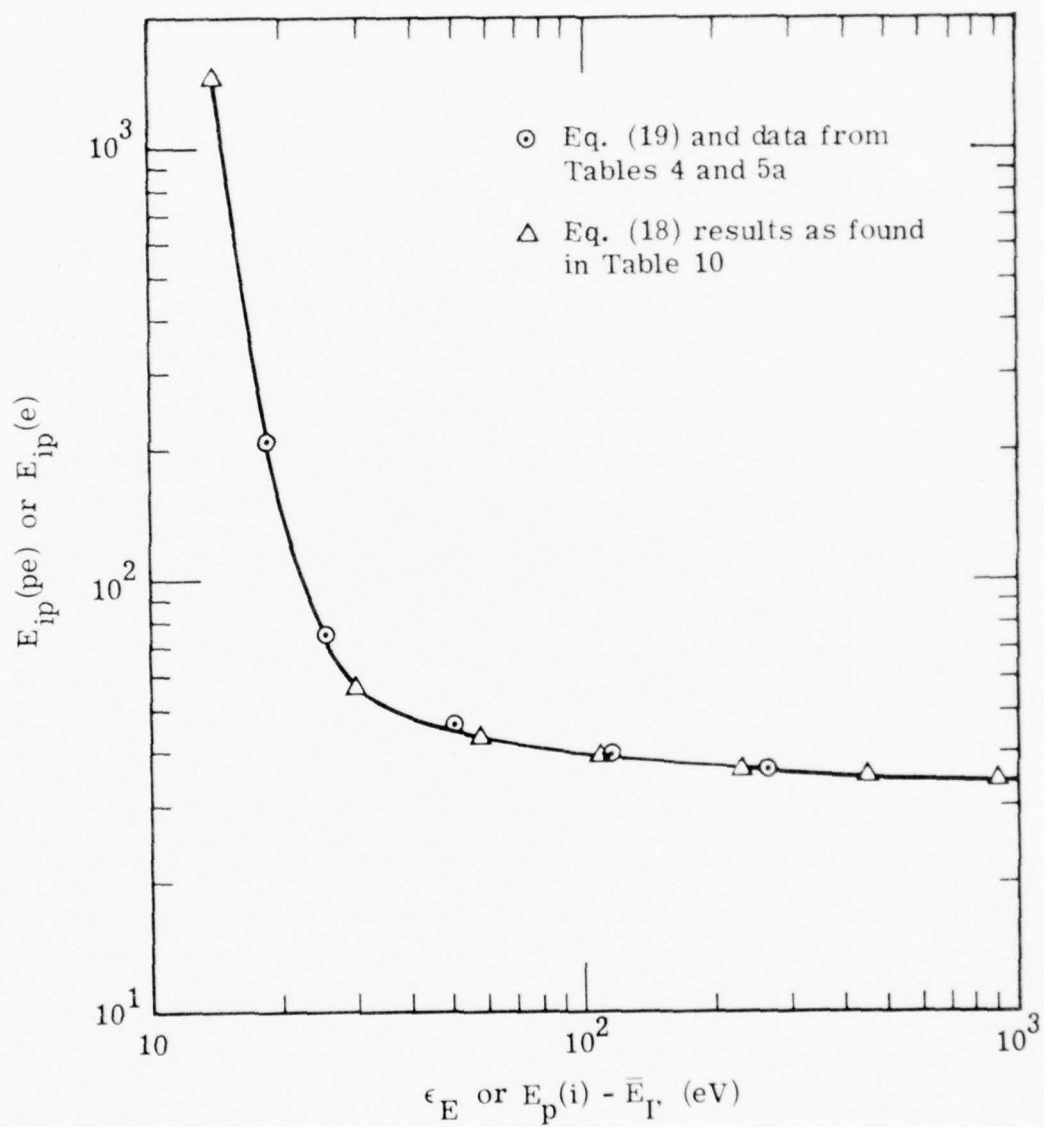


Figure 2. Comparison Between Electron Volts per Ion-Pair Resulting from Deposition of Photoelectron and Incident Electron.

2.3.3 Electron Flux Spectra

The electron flux spectra have been calculated by using the steady state densities of electrons in each electron energy bin according to the equation [MS-75]

$$\psi = v_j [e_j] / \Delta U_j \quad (20)$$

where ψ is the flux and ΔU_j the width of energy bin j .

The relative contributions of the thermal electrons and photoelectrons to the electron flux spectra over the range of photon energies and altitudes considered here, vary. At 60 and 110 km, the photoelectron contribution is greatly in excess of the thermal electron contribution for photon energies above 12.51 eV. The photoelectron contribution dominates at higher altitudes for photon energies (and for electron bin energies) above 14.84 (2.9), 15.74 (3.6), and 17.63 (5.7) eV at altitudes of 145, 250, and 500 km, respectively. The electron flux spectra presented here will include the photoelectron contribution but not the thermal electron contribution; the latter can be readily added to the spectra, if desired [MH-75a].

A typical electron flux spectrum at 60 km is shown in Figure 3 for a photon energy of 20.67 eV. For lower photon energies, the spectrum would be similar to that in Figure 3 but terminated at a lower electron bin energy; for higher photon energies, the decline in flux for higher electron bin energies would be extended to higher energies (note that the electron energy scale of Figure 3 is a logarithmic scale). The electron flux spectrum is essentially that shown and discussed previously [MS-75] for electron energy deposition.

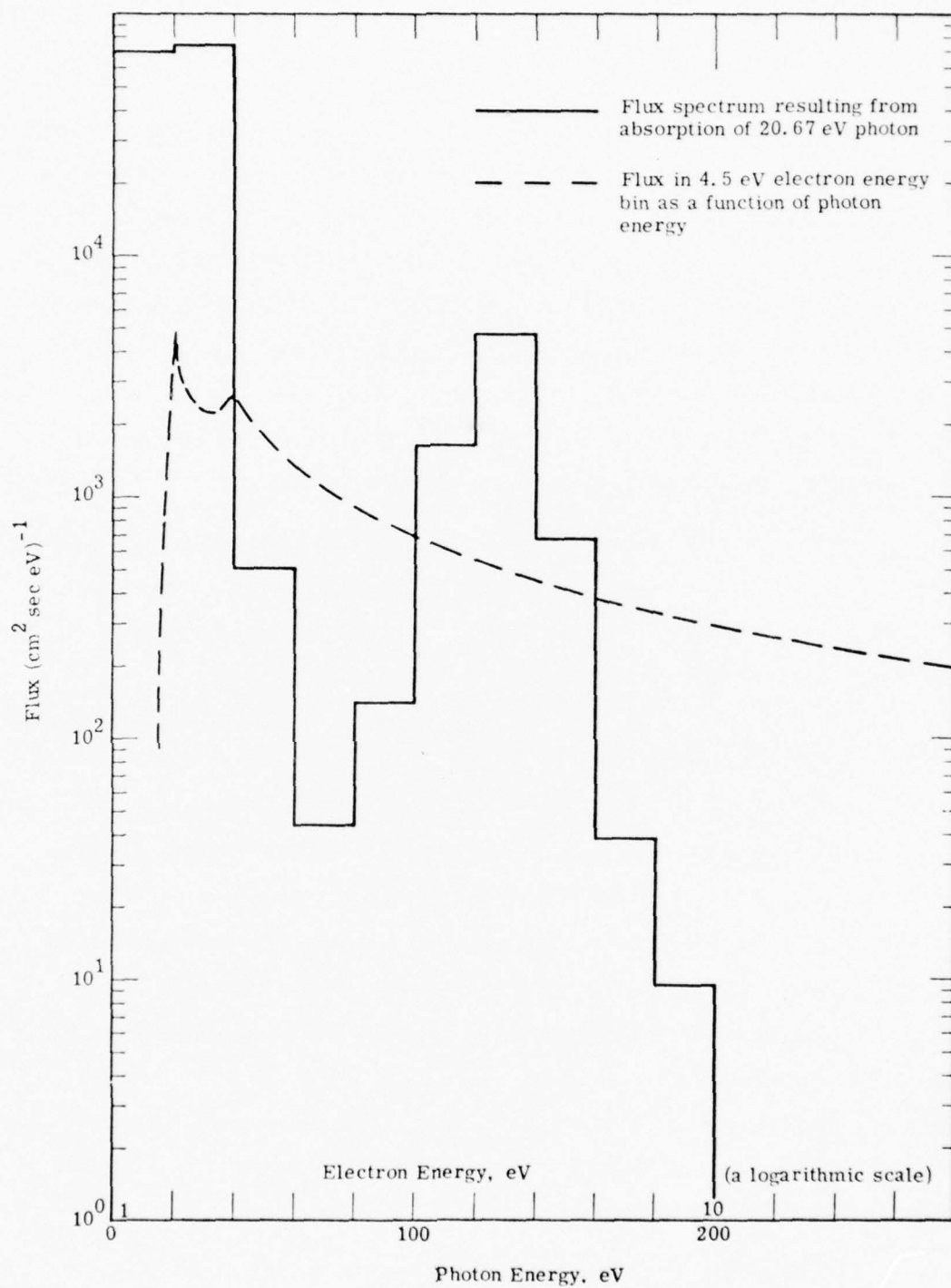


Figure 3. Electron Flux Spectrum and Dependence of Flux on Photon Energy at 60 km.

Also shown in Figure 3 is the electron flux as a function of photon energy for the 4.5 eV electron energy bin. Maxima in the flux occur at 20.67 and 40.8 eV. This shape for the flux-photon energy profile persists (maxima at approximately the same photon energy) for other electron bin energies but with the profile terminated on the low-energy side at progressively higher photon energies for higher electron bin energies. This same shape and behavior are found in flux data at higher altitudes. At 250 km, for example, only the maxima are shifted to higher energies by several eV.

The change in the photoelectron contribution to the electron flux spectrum with altitude is shown in Figure 4 for 20.67 eV photons. The minimum, centered about 2.3 eV, vanishes with increase in altitude as previously discussed [MH-75a].

2.3.4 Disturbed Atmospheres

Calculations of the initial species, energy partitioning, electron flux spectra and derived quantities have been made for disturbed atmospheres. The disturbed atmospheres are represented in the calculations by using a background electron density in excess of the ambient electron density of the undistributed (natural) atmosphere. The basis of the selection of the range of these background electron densities has been given in Section 2.2.4 above. Because of the extensiveness of these calculations only a summary is given here; details must be obtained by examining the microfiche for the calculations (see Appendix A).

The effect of increasing the background ionization is to increase the Coulomb interactions between the thermal subset of electrons (the background electrons) and the high-energy subset of

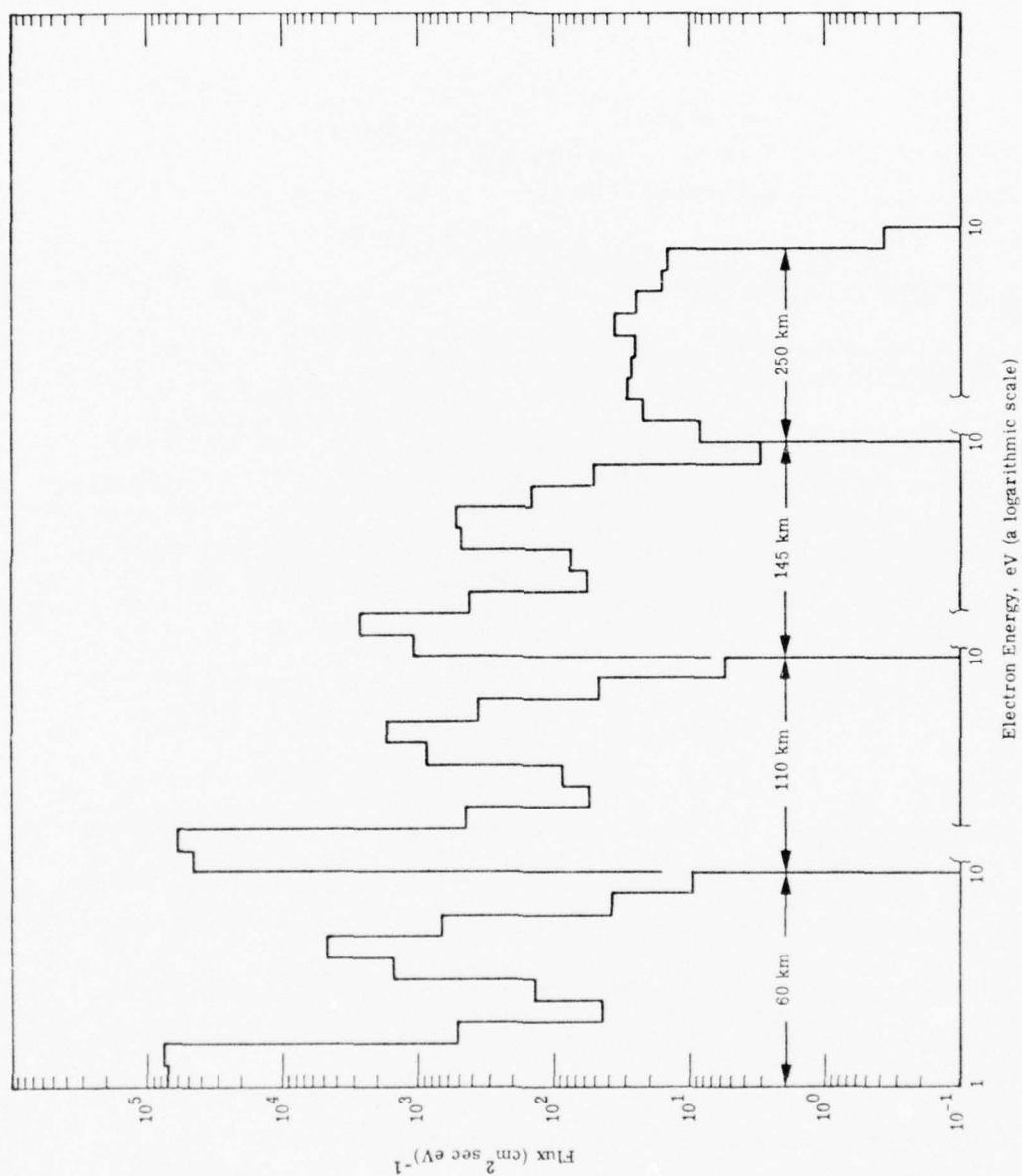


Figure 4. Photoelectron Flux Spectra from Absorption of 20.67 eV Photons at Various Altitudes (photon flux, $\phi = 10^3$ photons/cm² sec for all altitudes).

electrons. This reduces the number of high-energy electrons in progressively higher energy bins as the background electron density is increased. In turn, this reduces the occurrence of processes with progressively higher energy requirements.

In the present calculations, background electron densities were raised by factors of 10^{12} at 60 km and by 10^4 at all other altitudes. At 60 km, no effect on species densities was found until the background density exceeded the ambient density by factors of 10^8 or larger. Positive ion densities were not affected by the increased background electron densities at any altitude for photon energies less than 33.67 eV; for photon energies at and above 33.67 eV, reductions in the positive ion densities by 5 - 40% and 5 - 90% at 145 and 250 km, respectively, were found. Since the electron densities at and above 33.67 eV are relatively small, the overall effect on positive ion densities of the increased background electron densities is negligible. The neutral species derived from photoabsorption are decreased with increasing background electron density by factors greater than 100, 5, and 1.3 at altitudes of 250, 145, and 110 km, respectively, and by 30% or less at 60 km. The exceptions to these changes are nitrogen atoms (which are decreased only by factors of 1.1 to 3 at 145 km and negligibly at 110 km) and $O_2(a)$ and $O_2(b)$ (which are decreased by factors of 10 - 20 at 60 km).

The changes in the energy partitioning with increasing background electron densities at 60 and 110 km consist in an increase in the fractional energy of the electron translational mode by up to 0.12 and a concomitant decrease in fraction of energy in vibrational and electronic excitation modes. At 145 and 250 km, the changes upon absorption of photons with energies less than about 20 eV, are negligible

in all energy modes. At higher photon energies, the fractional energy in the electron translational mode increases (by up to 0.3 and 0.75 at altitudes of 145 and 250 km, respectively) and the fraction of energy in the electronic excitation, radiation and ionization modes decreases.

The change in the electron flux spectrum with increasing background electron density is shown in Figure 5 for the case of absorption at 145 km of photons with energy of 20.67 eV. The flux shown consists only of the photoelectron contribution; the arrows indicate the energy above which the photoelectron contribution is greater than the thermal (background) electron contribution. As shown in Figure 5, the electron flux is preferentially reduced in the low-energy bins; however, the more important reduction is that in the higher energy bins since the thermal (background) electron flux for the low-energy bins is much greater than the photoelectron flux. The flux spectra at different background electron densities will tend to merge in higher electron energy bins in the case of absorption of high-energy photons.

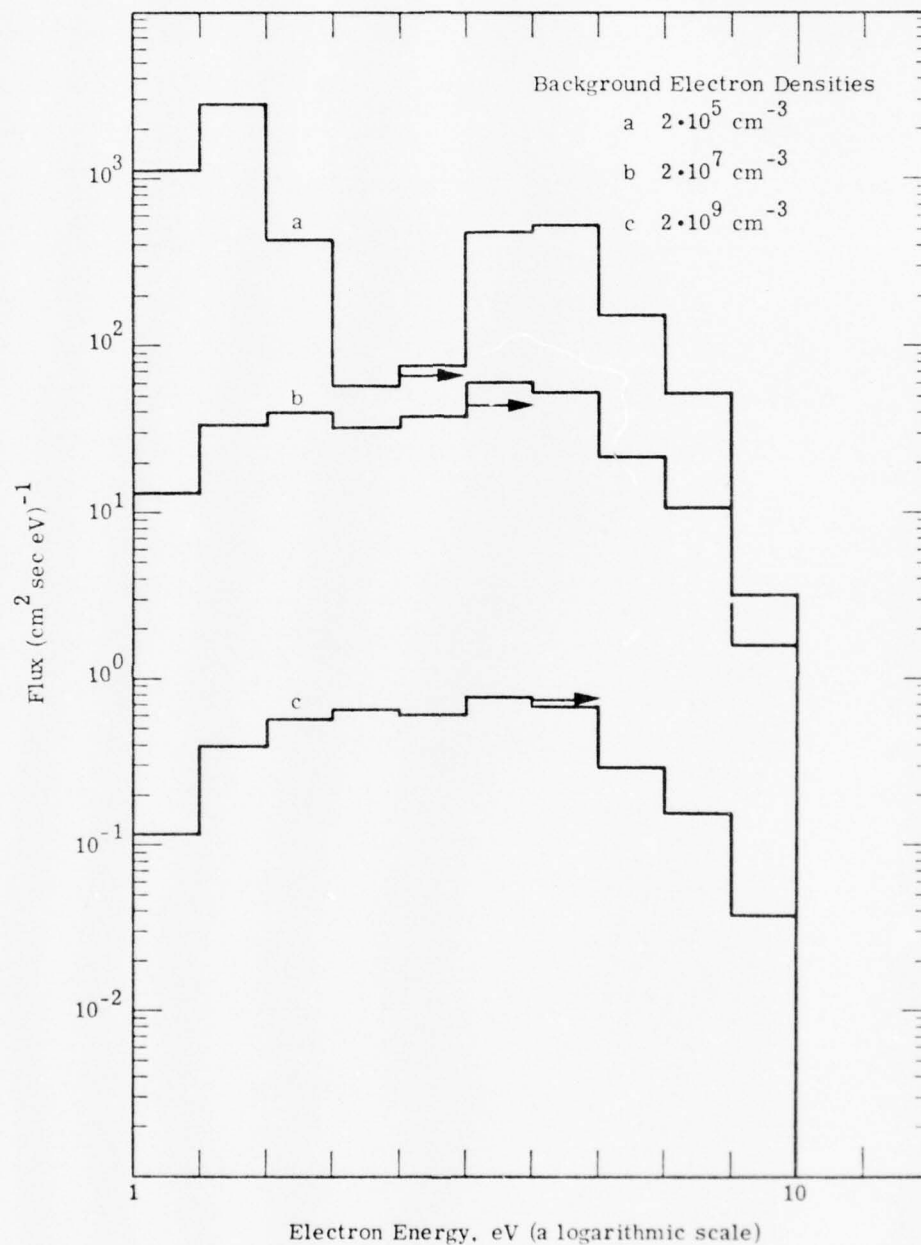


Figure 5. Electron Flux Spectra at 145 km for Various Background Electron Densities Following Absorption of 20.67 eV Photons. (See text for significance of arrows.)

3. ELECTRON ENERGY DEPOSITION

The species and energy densities which result from the deposition of electrons in the earth's atmosphere are calculated. These calculations are, to a large extent, a repetition of previous calculations [MS-75] but with the changes and additions indicated in Sections 2.2 and 4. An added feature of the present calculations is inclusion of electron deposition in disturbed atmospheres — the latter being defined as in Section 2.3.4.

The method of calculation for species and energy densities and derived quantities has been discussed elsewhere [MS-75].

3.1 CONDITIONS OF THE CALCULATIONS

The input data for the calculations of electron deposition are given in Table 9. For each of sixteen electron densities, a series of calculations for the seven values of the initial electron energy, U , were made. The calculations spanned the same range of altitudes and atmospheric compositions as were used in the photon deposition calculations. See Section 2.2.4 for additional discussion of input data.

3.2 RESULTS

The results are presented of calculations with the ISRAD code for the deposition, in the ambient and disturbed atmosphere, of electrons with energies in the range 14 to 900 eV and at altitudes in the range 60 to 500 km.

Table 9. Input Data for Electron Deposition Calculations*.

Alt, km	60	110	145	250	-	-	-
$[N_2], \text{ cm}^{-3}$	5.21(15)	1.58(12)	3.78(10)	4.35(8)	1.0(8)	5.21(15)	1.0(10)
$[O_2], \text{ cm}^{-3}$	1.40(15)	2.50(11)	4.21(9)	2.74(7)	1.0(8)	1.0(10)	1.4(15)
$[O], \text{ cm}^{-3}$	2.0(10)	3.23(11)	2.98(10)	1.91(9)	2.5(13)	1.0(10)	1.0(10)
$\theta_v, \text{ eV}$	0.0215	0.0211	0.0607	0.1105	0.122	0.0215	0.0215
$\theta, \text{ eV}$	0.0215	0.0221	0.0847	0.1656	0.218	0.0215	0.0215
T, eV	0.0215	0.0211	0.0607	0.1105	0.122	0.0215	0.0215
$[e], \text{ cm}^{-3}$	1.0(1)	1.0(5)	2.0(5)	6.3(5)	2.6(5)	1.0(5)	1.0(5)
and	1.0(8)	1.0(7)	2.0(7)	6.3(7)			
$[NO^+], \text{ cm}^{-3}$	1.0(10)	1.0(9)	2.0(9)	6.3(9)			
	1.0(12)						

*U, eV = 900, 450, 230, 110, 57, 29, 14, for each column.

3.2.1 Initial Species

The initial species formed by the deposition of electrons with initial energies in the range 14 to 900 eV are listed in Table 10 in terms of the number of particles formed per ion pair. These quantities were calculated as previously described [MS-75]. The species listed in Tables 10a through 10d correspond to electron absorptions at altitudes of 60, 110, 145, and 250 km, respectively; those listed in Tables 10e, 10f, and 10g correspond to electron absorption in single component gases of molecular oxygen, molecular nitrogen and atomic oxygen, respectively, with background electron densities. The atomic oxygen case, Table 10g, may be regarded as a 500 km altitude calculation as indicated in Section 2.3.1.

The only significant difference between the results of the present calculation and the previous calculation [MS-75] in terms of initial species is in the atomic nitrogen densities. Because of the reanalysis of the electron impact excitation and dissociation (and predissociation) of molecular nitrogen as presented in Section 4, the nitrogen atom densities are smaller in the present calculations. The $N(^4S^o)$ densities are found to be about 40% and the $N(^2D^o)$ densities to be about 45% of the previously calculated [MS-75] values at altitudes from 60 through 145 km.

3.2.2 Energy Partitioning

The partitioning of energy into seven modes is shown on Table 11; as before (see MS-75 and Section 2.3.2 above) the values listed in the table are the fractions of the total energy appearing in mode M. Table 11a contains data on energy partitioning for various

Tables 10a and 10b. Species Densities per Ion-Pair at 60 and 110 km and Ambient Electron Density.

Table 10a

Table 10b

U, eV	Altitude = 60 km; [e] _{amb} = 10 cm ⁻³						Altitude 110 km; [e] _{amb} = 1.0 × 10 ⁵ cm ⁻³							
	900	450	230	110	57	29	14	900	450	230	110	57	29	14
O(³ P)	0.228	0.233	0.261	0.313	0.408	0.673	15.47	0.179	0.186	0.204	0.246	0.322	0.532	15.11
O(¹ D)	0.126	0.134	0.143	0.181	0.239	0.386	6.335	0.558	0.586	0.635	0.730	0.926	1.362	86.54
O(¹ S)	-	-	-	-	-	-	-	0.014	0.015	0.016	0.019	0.024	0.036	1.741
O(⁴ S ^o)	0.072	0.075	0.071	0.059	0.040	0.016	-	0.082	0.086	0.088	0.088	0.088	0.103	0.476
O(² D ^o)	-	-	-	-	-	-	-	0.055	0.053	0.060	0.063	0.068	0.080	-
O ₂ (¹ Δ _g)	0.767	0.805	0.869	1.000	1.273	1.925	133.7	0.271	0.283	0.304	0.351	0.446	0.680	36.10
O ₂ (¹ Σ _g ⁺)	0.114	0.121	0.131	0.149	0.188	0.266	24.12	0.032	0.034	0.036	0.041	0.052	0.074	5.143
O ₂ (¹ Σ _g ⁻)	0.160	0.154	0.154	0.159	0.171	0.191	1.000	0.094	0.090	0.089	0.090	0.095	0.101	0.524
O ₂ (² Π _g)	0.016	0.017	0.019	0.021	0.027	0.035	2.786	0.005	0.006	0.006	0.007	0.009	0.012	0.685
O ₂ (² P)	0.198	0.215	0.234	0.250	0.230	0.162	1.072	0.199	0.214	0.230	0.242	0.218	0.146	0.955
N(⁴ S ^o)	0.241	0.264	0.291	0.317	0.290	0.181	1.072	0.242	0.263	0.287	0.308	0.276	0.162	0.955
N(² D ^o)	0.226	0.244	0.267	0.292	0.287	0.247	1.311	0.225	0.241	0.262	0.283	0.272	0.222	1.167
N(² D ^o)	0.290	0.317	0.353	0.392	0.378	0.275	1.311	0.290	0.315	0.348	0.381	0.358	0.247	1.167
N(² P ^o)	0.001	0.002	0.002	0.002	0.002	0.001	-	0.001	0.002	0.002	0.002	0.002	0.001	-
N ₂ (³ Λ _u ⁻)	0.591	0.597	0.635	0.772	1.050	2.037	76.88	0.538	0.543	0.578	0.701	0.945	1.781	68.39
N ₂ (¹ Π _g)	0.113	0.116	0.128	0.162	0.229	0.457	19.15	0.103	0.106	0.117	0.148	0.208	0.399	17.09
N(³ P)	0.139	0.145	0.142	0.121	0.077	0.006	-	0.141	0.146	0.141	0.119	0.074	0.006	-
N ₂ (¹ Σ _g ⁺)	0.628	0.626	0.633	0.661	0.712	0.784	-	0.628	0.620	0.623	0.640	0.674	0.710	-

Tables 10c and 10d. Species Densities per Ion-Pair at 145 and 250 km and Ambient Electron Density.

Table 10c

U, eV	Altitude = 145 km; $[e]_{\text{amb}} = 2.0 \times 10^5 \text{ cm}^{-3}$						Altitude = 250 km; $[e]_{\text{amb}} = 6.3 \times 10^5 \text{ cm}^{-3}$							
	900	450	230	110	57	29	14	960	450	230	110	57	29	14
$O(^3P)$	0.231	0.237	0.260	0.312	0.408	0.652	15.87	0.363	0.363	0.394	0.467	0.601	0.895	17.48
$O(^1D)$	0.787	0.814	0.869	1.004	1.262	1.884	53.47	0.385	0.396	0.418	0.480	0.592	0.914	12.45
$O(^1S)$	0.027	0.028	0.029	0.035	0.044	0.068	1.370	0.024	0.024	0.026	0.030	0.038	0.060	1.013
$O(^4S^o)$	0.145	0.152	0.161	0.177	0.198	0.252	0.832	0.285	0.295	0.311	0.343	0.377	0.447	0.980
$O(^2D^o)$	0.171	0.180	0.182	0.187	0.196	0.210	-	0.419	0.426	0.421	0.411	0.404	0.384	-
$O_2(a^1\Delta_g)$	0.044	0.045	0.048	0.055	0.069	0.103	2.707	0.002	0.002	0.002	0.003	0.003	0.005	0.057
$O_2(b^1\Sigma_g^-)$	0.009	0.009	0.010	0.011	0.014	0.021	0.574	-	-	-	0.001	0.001	0.001	0.013
$O_2^+(X^2\Pi_g)$	0.054	0.051	0.049	0.049	0.050	0.048	0.168	0.014	0.012	0.012	0.011	0.010	0.009	0.020
$O(^2P)$	0.002	0.002	0.002	0.002	0.002	0.004	0.070	-	-	-	-	-	-	0.001
$N(^4S^o)$	0.163	0.173	0.184	0.189	0.163	0.099	0.434	0.073	0.075	0.078	0.076	0.082	0.032	0.092
$N(^4S^o)$	0.198	0.212	0.229	0.240	0.206	0.111	0.434	0.089	0.092	0.097	0.097	0.078	0.036	0.092
$N(^2D^o)$	0.184	0.194	0.208	0.219	0.203	0.151	0.530	0.081	0.083	0.088	0.088	0.076	0.049	0.112
$N(^2D^o)$	0.237	0.253	0.277	0.296	0.268	0.163	0.530	0.106	0.109	0.117	0.119	0.101	0.055	0.112
$N(^2P^o)$	0.001	0.001	0.002	0.002	0.002	0.001	-	-	0.001	0.001	0.001	0.001	-	-
$N_2(A^3\Sigma_u^-)$	0.407	0.413	0.438	0.521	0.687	1.222	31.99	0.130	0.133	0.141	0.161	0.209	0.347	8.695
$N_2(a^1\Pi_g)$	0.077	0.078	0.087	0.109	0.150	0.270	7.836	0.027	0.027	0.030	0.037	0.050	0.084	1.783
$N^+(^3P)$	0.118	0.119	0.114	0.094	0.056	0.004	-	0.054	0.053	0.050	0.039	0.022	0.001	-
$N_2^+(X^2\Sigma_g^-)$	0.513	0.498	0.494	0.494	0.501	0.485	-	0.229	0.214	0.207	0.197	0.187	0.160	-

Table 10d

Tables 10e, f and g. Species Densities per Ion-Pair in Atomic Oxygen,
Molecular Oxygen and Molecular Nitrogen.

Tables 10e and 10f

Table 10g

U, eV	O_2 ; N_2 ; $[e]_{amb} = 1.0 \times 10^5 \text{ cm}^{-3}$							Atomic Oxygen; $[e]_{amb} = 2.6 \times 10^5 \text{ cm}^{-3}$						
	900	450	230	110	57	29	14	900	450	230	110	57	29	14
$O(^3P)$	1.600	1.633	1.723	2.029	2.591	4.487	17.43	0.526	0.520	0.559	0.639	0.802	1.129	17.13
$O(^1D)$	0.735	0.748	0.793	0.967	1.259	2.137	5.488	1.610	1.668	1.755	1.963	2.341	3.495	28.15
$O(^1S)$	-	-	-	-	-	-	-	0.065	0.068	0.071	0.080	0.095	0.144	0.961
$O(^4S)$	0.290	0.310	0.306	0.260	0.185	0.068	-	0.396	0.401	0.417	0.449	0.480	0.540	1.000
$O(^2D)$	-	-	-	-	-	-	-	0.604	0.599	0.583	0.551	0.520	0.460	-
$O_2(a^1\Delta_g)$	2.526	2.609	2.764	3.197	4.065	6.976	32.32	-	-	-	-	-	-	0.002
$O_2(b^1\Sigma_g^-)$	0.484	0.500	0.529	0.612	0.777	1.270	5.513	-	-	-	-	-	-	-
$O_2(X^2\Pi_g)$	0.710	0.690	0.694	0.741	0.816	0.933	1.000	-	-	-	-	-	-	-
$O(^2P)$	0.035	0.036	0.038	0.045	0.057	0.088	0.650	-	-	-	-	-	-	-
$N(^4S)$	0.258	0.279	0.300	0.319	0.290	0.202	-	-	-	-	-	-	-	-
$N(^4S)$	0.315	0.343	0.375	0.405	0.367	0.226	-	-	-	-	-	-	-	-
$N(^2D)$	0.292	0.314	0.343	0.372	0.362	0.308	-	-	-	-	-	-	-	-
$N(^2D)$	0.377	0.410	0.454	0.501	0.477	0.343	-	-	-	-	-	-	-	-
$N(^2P)$	0.001	0.002	0.003	0.003	0.003	0.002	-	-	-	-	-	-	-	-
$N_2(A^3\Sigma_u^-)$	0.698	0.708	0.760	0.938	1.282	2.415	-	-	-	-	-	-	-	-
$N_2(a^1\Pi_g)$	0.125	0.130	0.146	0.188	0.270	0.534	-	-	-	-	-	-	-	-
$N(^3P)$	0.185	0.191	0.184	0.156	0.098	0.008	-	-	-	-	-	-	-	-
$N_2(X^2\Sigma_g^-)$	0.815	0.809	0.816	0.844	0.902	0.902	-	-	-	-	-	-	-	-

Table 11a. Energy Partitioning for Varying Altitudes and Source Electron Flux Energies.

Alt, km	U, eV	Fractional Energy						
		900	450	230	110	57	29	14
60	f_K	0.050	0.051	0.050	0.044	0.033	0.016	0.010
	f_E	0.018	0.018	0.016	0.008	0.002	0.013	0.042
	f_R	0.161	0.166	0.177	0.193	0.210	0.226	0.237
	f_{X_v}	0.064	0.065	0.067	0.072	0.084	0.107	0.210
	f_I	0.427	0.415	0.398	0.372	0.339	0.262	0.008
	f_D	0.119	0.124	0.128	0.128	0.116	0.087	0.048
	f_{X_e}	0.161	0.160	0.165	0.182	0.215	0.288	0.446
	E_{ip}	34.5	35.5	37.1	39.8	43.7	56.7	1482.
100	f_K	0.043	0.044	0.043	0.037	0.027	0.010	0.005
	f_E	0.030	0.030	0.027	0.021	0.018	0.033	0.072
	f_R	0.169	0.175	0.186	0.203	0.222	0.243	0.282
	f_{X_v}	0.050	0.050	0.052	0.056	0.066	0.084	0.146
	f_I	0.435	0.423	0.407	0.382	0.351	0.277	0.009
	f_D	0.106	0.111	0.113	0.111	0.096	0.063	0.027
	f_{X_e}	0.166	0.167	0.171	0.188	0.220	0.289	0.459
	E_{ip}	34.1	35.0	36.4	38.9	42.3	53.5	1407.
145	f_K	0.035	0.035	0.034	0.029	0.020	0.006	0.002
	f_E	0.046	0.046	0.044	0.040	0.040	0.062	0.119
	f_R	0.181	0.184	0.196	0.215	0.237	0.265	0.362
	f_{X_v}	0.035	0.036	0.037	0.040	0.046	0.059	0.101
	f_I	0.450	0.441	0.426	0.403	0.372	0.301	0.016
	f_D	0.086	0.089	0.091	0.087	0.072	0.041	0.016
	f_{X_e}	0.166	0.168	0.172	0.186	0.212	0.267	0.385
	E_{ip}	32.5	33.2	34.3	36.3	39.2	48.2	813.
250	f_K	0.016	0.016	0.016	0.013	0.008	0.002	0.001
	f_E	0.142	0.145	0.147	0.152	0.167	0.221	0.312
	f_R	0.190	0.189	0.200	0.221	0.251	0.284	0.462
	f_{X_v}	0.008	0.009	0.009	0.009	0.010	0.013	0.022
	f_I	0.483	0.478	0.466	0.444	0.408	0.330	0.028
	f_D	0.040	0.041	0.041	0.038	0.028	0.013	0.004
	f_{X_e}	0.120	0.122	0.122	0.123	0.128	0.137	0.170
	E_{ip}	29.2	29.4	30.2	31.6	34.3	42.2	485.

Table 11b. Energy Partitioning for Single Constituent Gases and Varying Source Electron Flux Energies.

Gas	U, eV	Fractional Energy						
		900	450	230	110	57	29	14
O	f_K	-	-	-	-	-	-	-
	f_E	0.044	0.045	0.046	0.042	0.046	0.072	0.111
	f_R	0.222	0.219	0.230	0.253	0.290	0.330	0.644
	f_{X_v}	-	-	-	0.001	0.001	0.001	-
	f_I	0.515	0.514	0.502	0.481	0.439	0.356	0.046
	f_D	-	-	-	-	-	-	-
	f_{X_e}	0.219	0.222	0.221	0.223	0.225	0.241	0.199
	E_{ip}	26.4	26.5	27.1	28.3	31.0	38.2	297
N ₂	f_K	0.041	0.042	0.041	0.036	0.024	0.005	0.000
	f_E	0.036	0.035	0.032	0.027	0.022	0.039	0.079
	f_R	0.171	0.177	0.190	0.207	0.225	0.244	0.258
	f_{X_v}	0.072	0.073	0.076	0.080	0.095	0.119	0.308
	f_I	0.429	0.416	0.399	0.373	0.344	0.272	-
	f_D	0.110	0.114	0.117	0.113	0.092	0.047	0.009
	f_{X_e}	0.141	0.143	0.145	0.164	0.198	0.274	0.346
	E_{ip}	35.9	36.9	38.5	41.3	45.0	57.2	-
O ₂	f_K	0.096	0.098	0.096	0.090	0.081	0.074	0.087
	f_E	-	-	-	-	-	-	0.028
	f_R	0.086	0.088	0.092	0.106	0.114	0.110	0.035
	f_{X_v}	0.003	0.003	0.003	0.003	0.004	0.005	0.006
	f_I	0.421	0.413	0.398	0.372	0.326	0.234	0.082
	f_D	0.228	0.228	0.231	0.250	0.274	0.331	0.403
	f_{X_e}	0.116	0.170	0.180	0.179	0.201	0.246	0.359
	E_{ip}	29.7	30.3	31.5	33.5	37.9	52.1	147.

source electron flux energies as a function of altitude; Table 11b has data on single component gases.

The major differences between the present and previous [MS-75] calculations of energy partitioning arise from a reduction in energy in dissociation and an increase in the energy in radiation. These changes approach a factor of two in magnitude; they result from the reassessment of the extent of predissociation of nitrogen, this being smaller in the present calculations. Also, the electron volts per ion pair is generally smaller in the present calculations.

3.2.3 Loss Functions

The loss functions, calculated according to Eq. (20) of MS-75, are shown in Figure 6.

3.2.4 Electron Flux Spectra

The electron flux spectra calculated here are not sufficiently different from those previously calculated [MS-75] to warrant discussion.

3.2.5 Disturbed Atmospheres

The calculation of the initial species, energy partitioning, electron flux spectra and derived quantities was performed for electron deposition in a similar manner as for photon deposition except that at each altitude the variation in energy represented the initial electron energy over the range 900 to 14 eV. The general effect on these calculations of the increased background ionization in disturbed atmospheres has been discussed above (see Section 2.3.4). Also,

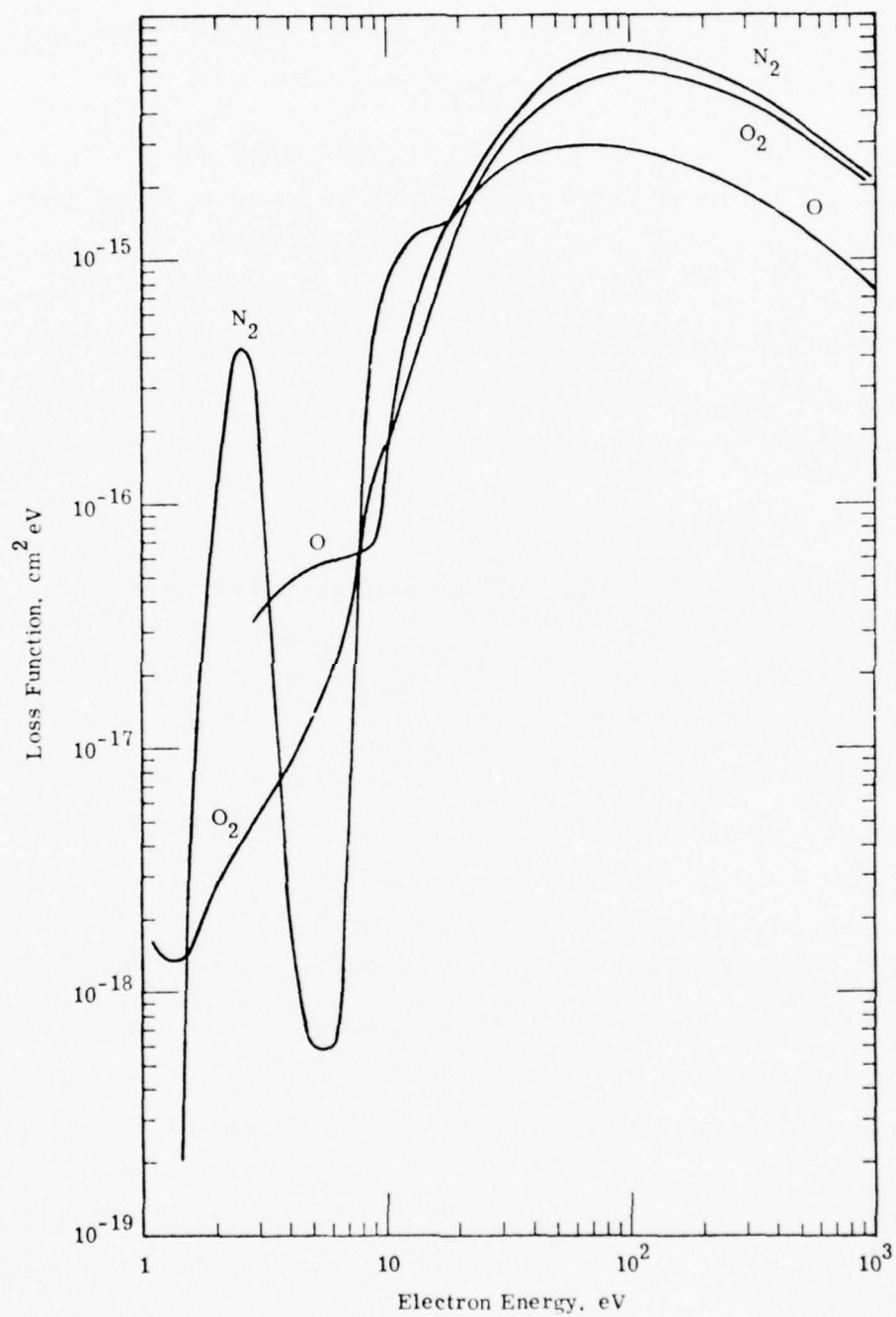


Figure 6. Loss Functions for N_2 , O_2 and O .

as before, the background electron densities in the present calculations were raised above the ambient values by factors of 10^{12} at 60 km and by 10^4 at all other altitudes. Only a summary of the results of the calculations is presented below.

At 60 km, no effect on species densities was found until the background electron density exceeded the ambient electron density by a factor of greater than 10^8 . The positive ion densities were essentially unaffected by the increased background electron densities at all altitudes; at higher altitudes, 145 and 250 km where small changes did occur, the positive ion densities decreased by less than 10%. The densities of the neutral species decreased with increase in the background ionization except for the nitrogen atoms, $N(^4S^\circ)$, $N(^2D^\circ)$, and $N(^2P^\circ)$, whose densities did not change either with background electron density or with altitude. The factors by which the neutral species densities decreased were less than about 50, 20, 5, and 1.2 at altitudes of 250, 145, 110, and 60 km, respectively, except for $O_2(a^1\Delta_g)$ and $O_2(b^1\Sigma_g^+)$ which experienced greater decreases at the lower altitudes. At a given altitude, the decreases in neutral species densities were smaller at smaller initial electron energies.

The changes in the energy partitioning at 60 and 110 km consist only of an increase of the fraction of the energy in the electron translational mode and a corresponding decrease in the vibrational and electronic excitation modes when the background electron density is increased; all other energy modes are unchanged. At higher altitudes, the principal changes are the same as at 60 and 110 km but the fractions of the total energy in other energy modes decrease

with increasing background electron density. At a given altitude, the magnitude of the change in any energy mode increases with decrease in the initial electron energy.

The changes in the electron flux spectra with increase in the background electron density have the same general features as found in the case of photon absorption (see Section 2.3.4). The electron flux is preferentially reduced in the low-energy bins, the shape of the high-energy electron contribution to the flux spectra changes in general as shown in Figure 5 and the flux spectra for different background electron densities merge for the high-energy electron energy bins.

4. EXCITATION TO PREDISSOCIATING STATES OF NITROGEN

In previous calculations [MS-75] of the initial species formed after absorption of electrons in the atmosphere, the largest uncertainty in the species densities was associated with nitrogen atoms. This uncertainty was related to the extent of predissociation assigned to specific excited states of nitrogen and to the excitation cross-section values employed in the calculations. In this section, these aspects of treating nitrogen atom formation are reviewed and new values of fractional predissociation and excitation cross-sections are obtained. The cross-section values are derived in a consistent manner by combining data available in the literature and lead, in calculations of electron energy degradation, to the observed value of the energy per ion pair formed in nitrogen.

4.1 PREDISSOCIATION OF NITROGEN

The states of nitrogen which have been considered in accounting for predissociation consist of the valence states $b\ ^1\Pi_u$ and $b'\ ^1\Sigma_u^+$ and the Rydberg states $c_n'\ ^1\Sigma_u^+$, $c_n\ ^1\Pi_u$, $o_n\ ^1\Pi_u$, and $a_n''\ ^1\Sigma_g^+$ where $n \geq 3$ (using the principal quantum numbers assignments of LD-72). The first five listed states apparently are the principal states contributing to nitrogen atom formation. The evidence for predissociation and the product states is considered first; then estimates of the extent of predissociation are made.

For the $b\ ^1\Pi_u$ state, levels $v = 0, 2, 3$, and 4 are predissociated [CC-69] while levels $v = 1, 5$, and 6 are not. For levels above $v = 6$ there is a possibility of predissociation but no firm

evidence for it. The present calculations will include predissociation in the levels above $v = 6$ but this does not represent an important assumption since the excitation to levels $v \leq 6$ accounts for about 83% of the excitation. The $b^1\Pi_u$ state most probably predissociates to the product-pair, $N(^4S^\circ) + N(^2D^\circ)$ [CC-69]; this product-pair is adopted here.

For the $b'^1\Sigma_u^+$ state, there is an important uncertainty as to the occurrence of predissociation. Levels $v = 0$ to 9 have been observed in emission [CC-69] and levels $v = 20, 21$, and 22 are known [CC-70b] to be predissociated. There are apparently no data for the levels $v = 10$ through 19. Unfortunately, the latter group of vibrational levels are the most important for electron excitation based both on high-energy [GS-69d] and low-energy [La-69] electron loss spectra. For the results reported in Sections 2 and 3 above, repeat calculations were made by considering predissociation and no predissociation in levels $v = 10$ through 19 (see Sections 2.3.1 and 3.2.1). The products of predissociation will be taken as $N(^2D^\circ) + N(^2D^\circ)$ for levels $v \geq 20$ [CC-70b] and as $N(^4S^\circ) + N(^2D^\circ)$ for levels $v < 20$. Thus, as considered below, about 80% of the predissociated molecules lead to the product pair $N(^4S^\circ) + N(^2D^\circ)$.

The states $c'_n{}^1\Sigma_u^+$ are the first members of the Worley-Jenkins Rydberg series converging to the ground state of the nitrogen molecular ion. The principal quantum number of the lowest energy state has been given different assignments by different investigators; $n = 3$ according to LD-72 and $n = 4$ according to CY-72a. Here, $n = 3$ will be arbitrarily chosen. Following excitation to vibrational levels $v = 0, 1, 2, 3, 4$ of the lowest energy state $c'_3{}^1\Sigma_u^+$,

the energy of excitation is radiated [AD-71, CC-69]. (Excitation to the $v = 0$ level yields the most intense peak in the energy loss spectrum for 25 keV electrons [GS-69d].) Thus these vibrational levels are not important for predissociation. The higher vibrational levels, $v \geq 5$, are not recorded as being observed in emission [CC-69] and the rotational linewidths for $v = 5$ are possibly widened [CA-72], indicating the possibility of predissociation. The assumption of predissociation will be made for vibrational levels $v = 5, 6$, and 7 ; levels above $v = 7$ can be neglected in considering electron excitation processes. For the $c'_4 \Sigma_u^+$ state, electron excitation to the $v = 0$ and 1 levels is important and the more important of these levels, $v = 0$, is definitely predissociated [CC-70b]; level $v = 1$ will also be considered as predissociated. The products of predissociation are taken as $N(^4S^\circ) + N(^2D^\circ)$ for the $c'_3 \Sigma_u^+$ levels and as $N(^4S^\circ) + N(^2D^\circ)$ and $N(^2D^\circ) + N(^2D^\circ)$ for the $c'_4 \Sigma_u^+$ levels, respectively, to the extent of 82% and 18% on the basis of energy considerations. States with $n \geq 5$ will be treated below, together with states of $c_n \Pi_u$ having these principal quantum numbers.

The states $c_n \Pi_u$ are a Rydberg series which also converge to the ground state of the nitrogen molecular ion. For the lowest state, $c_3 \Pi_u$, vibrational levels $v = 1, 3$, and 4 are apparently predissociated [Dr-69]; the other vibrational levels of importance (essentially only $v = 0, 2$) will be regarded as not predissociating. The products of predissociation will be $N(^4S^\circ) + N(^2D^\circ)$ [Dr-69]. For the next lowest state, $c_4 \Pi_u$, only the $v = 0$ level has been observed in emission [CY-72a]; the other levels of interest in

connection with electron excitation, $v = 1$ and 2 , are regarded as being predissociated and as yielding the product pair $N(^2D^\circ) + N(^2D^\circ)$.

The states of $c'_n \ ^1\Sigma_u^+$ and $c_n \ ^1\Pi_u$ above $n = 4$ are considered together and without distinguishing vibrational levels. For $n = 7, 9$, and 12 , predissociation is observed [CY-72a] and for all higher states ($n > 4$) predissociation is probable. Here we recognize predissociation for states with $n = 7, 9$, and 11 through 24 and take the product pair to be $N(^2D^\circ) + N(^2D^\circ)$ [CY-72a].

For the $o_3 \ ^1\Pi_u$ state, no predissociation is reported in levels $v = 0, 1, 2, 3$, and 4 . For the $o_4 \ ^1\Pi_u$, only the $v = 1$ level is taken to be predissociated and with products $N(^2D^\circ) + N(^2D^\circ)$ [YT-75].

The $a'' \ ^1\Sigma_g^+$ Rydberg state is assumed to predissociate yielding $N(^4S^\circ) + N(^2D^\circ)$; there is no compelling evidence for these assumptions; however, the assumptions have little impact on the calculations since the excitation cross-section for the $a'' \ ^1\Sigma_g^+$ state is relatively small, accounting for not more than 1% of the total excitation cross-section.

In making estimates of the fractional predissociation resulting from excitation to a specific excited electronic state of nitrogen, use has been made of optical oscillator strengths and of intensities observed in the electron impact energy loss spectra. The fractional predissociation is the fraction of the total number of molecules, excited to the specific electronic state, which predissociate; the number of molecules excited to specific vibrational levels of the electronic state is assumed to be proportional to the

oscillator strength (which is valid for small collision vectors [Be-30]) or the intensity. Strictly, to use oscillator strengths and intensities on a comparable basis, corrections for excitation energy and angular resolution in the electron loss measurement must be made; however, these corrections are neglected here. The energy correction is small compared to other uncertainties since only one electronic state is being considered in each case and the energy spread of the relevant vibrational levels is relatively small; the angular resolution is assumed not to change over the small energy intervals encountered. The optical oscillator strength data [Ca-72] and the electron loss spectra intensities [GS-69d] yield the fractional predissociation (f_p) values shown in Table 12. The fourth column of Table 12 gives the selected range (Δf_p) or the average value (\bar{f}_p) of the fractional predissociation. The rationale for the selection of an average value from the data for the $b\ ^1\Pi_u$ state and the retention of the range for the $b'\ ^1\Sigma_u^+$ state is given below.

4.2 EXCITATION CROSS-SECTIONS

Absolute electron impact excitation cross-sections for the predissociating states of nitrogen being considered have not been measured individually. Here, these curves are derived by the following procedure. Measured values of relative cross-sections [BT-70b] are adjusted on the basis of absolute values for the $N_2(a\ ^1\Pi_g)$ state [Ho-69b, Bo-72] to obtain absolute values for the total cross-section curve for excitation to predissociating states. This procedure is possible for energies up to 80 eV; beyond this energy, the total cross-section curve is extended on the basis of

Table 12. Fractional Predissociation (f_p) for
Excited Electronic States of Nitrogen

State	f_p (CA-72)	f_p (GS-69d)	Δf_p or \bar{f}_p
$b \ ^1\Pi_u$	0.65 - 0.94	0.74 - 0.91	0.83
$b' \ ^1\Sigma_u^+$	0.18 - 0.94	0.12 - 0.94	0.18 - 0.94
$c_3 \ ^1\Pi_u$	0.45	0.48	0.46
$c_4 \ ^1\Pi_u$	0.08	0.29	0.19
$c'_3 \ ^1\Sigma_u^+$	0.05	0.10	0.075
$c'_4 \ ^1\Sigma_u^+$	1.0	1.0	1.0
$c_n \ ^1\Pi_u + c'_n \ ^1\Sigma_u^+$	0.70	-	0.70
$o_3 \ ^1\Pi_u$	0.0	-	0.0
$o_4 \ ^1\Pi_u$	0.57	-	0.57

theoretically derived shapes of the cross-section curves for individual predissociating states and relative values of these curve segments based on oscillator strength data. Cross-section curves for excitation to specific predissociating states of nitrogen for energies above several hundred eV are then derived on the basis of the absolute, total cross-section curve values and the oscillator strength data. These cross-section curves are extended to lower energies on the basis of compatible theoretical and experimental results for Rydberg states and of preservation of the ratio of cross-section values for valence states at the lower energies.

4.2.1 Total Cross-section Values

Relative cross-section values for various sets of excited states of nitrogen have been obtained by Brinkmann and Trajmar [BT-70b]. These measurements cover the range of incident electron energies between 15 and 80 eV and the energy loss range between 6 and 19 eV for scattering angles up to 80° . These values were originally normalized on the basis of absolute measurements of the cross section for excitation to the $C^3\Pi_u$ state of nitrogen [BS-69]. For present purposes, a preferable means of normalization is use of the absolute cross-section data for excitation to the $a^1\Pi_g$ state of nitrogen [Ho-69b, Bo-72]. There are independent measurements of the cross section for the latter state in the range between 20 and 2000 eV; these measurements are in excellent accord; the cross sections for the $a^1\Pi_g$ state are larger at higher energies than those of the $C^3\Pi_u$ state and the ratio of the values for the states corresponding to the 12-17 eV energy loss range (the predissociating states

of nitrogen) to those of the $a^1\Pi_g$ state are more likely to be accurate; the $a^1\Pi_g$ relative cross-section data [BT-70b] have the same slope ($d\sigma/dE$) above 20 eV as do the experimental, absolute cross-section data for the $a^1\Pi_g$ state [Ho-69b, Bo-72]. The relative cross-section data for the $a^1\Pi_g$ state [BT-70b] have been normalized at 80 eV to the least-squares fit of the absolute data [Ho-69b, Bo-72] as shown on Fig. 7. Values of the cross section, as shown on Fig. 7, are given in Table 14 below.

The absolute total cross-sections for excitation to predissociating states is now determined from the product of the absolute cross-sections for the $a^1\Pi_g$ state and the ratio of cross sections for excitation to the predissociating states and the $a^1\Pi_g$ state. Data for relative cross-section values for the predissociating states were taken from SK-75 which contains data supplementary to the original presentation [BT-70b]. The relative cross-sections for excitation to the predissociating states are taken to be the sum of the curves labeled T12.4, T14.0, and T16.0 in SK-75. The absolute total cross sections obtained in this way for energies less than or equal to 80 eV are listed in Table 14 below.

To extend the total cross section curve to energies above 80 eV, the theoretical cross-section curves for individual states in the high energy range [CL-72, AD-71] are added and the resulting curve matched with the absolute value of the cross section at 80 eV determined as described in the preceding paragraph; the theoretical curves are added by applying weighting factors to the curve values at 1000 eV which are based on optical oscillator strength and electron

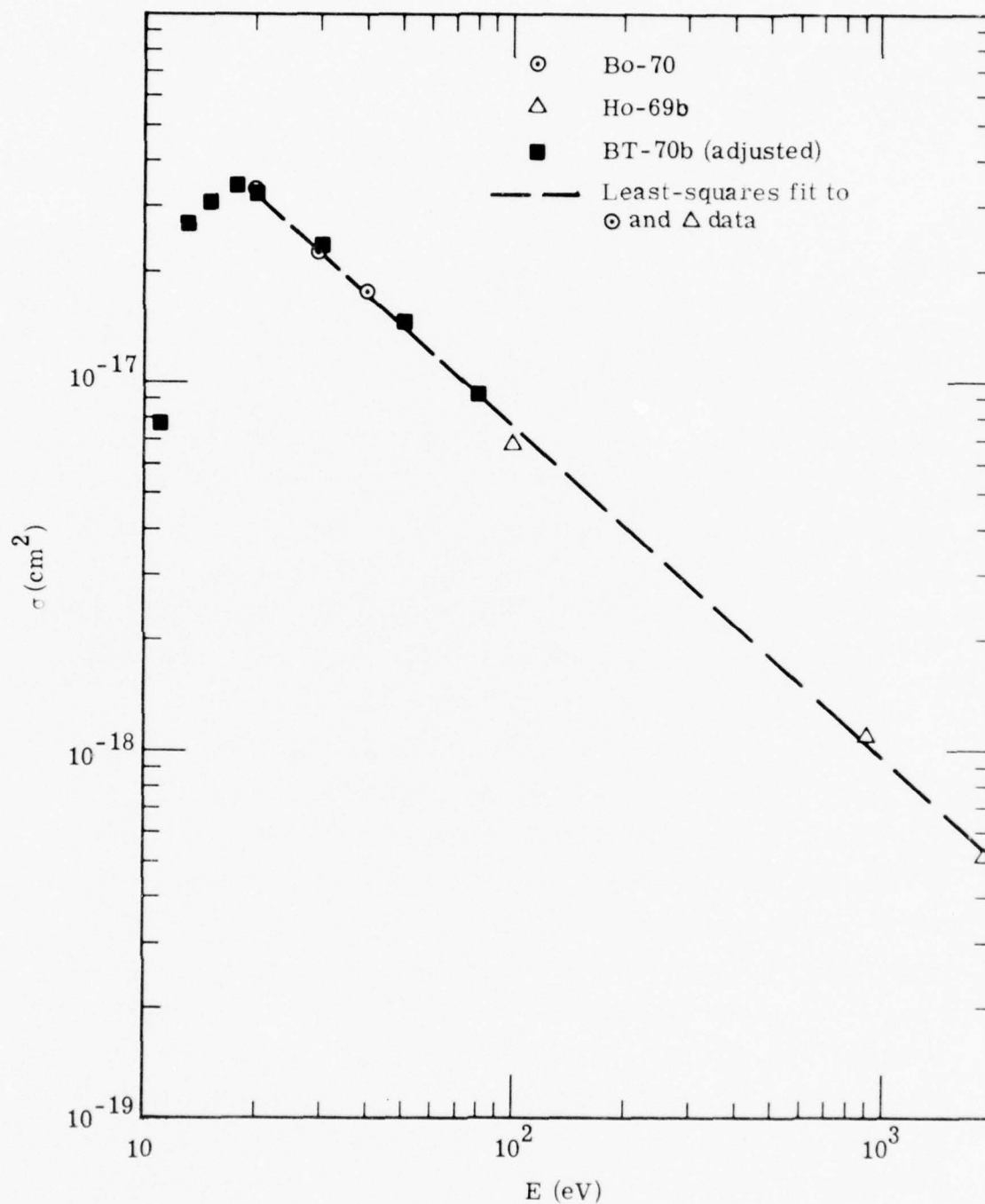


Figure 7. Cross-Section Curve for Excitation to $N_2(a^1\Pi_g)$:
Adjustment of Relative Cross-Section Data.

loss spectra intensity data. Thus, the absolute cross-section for energies above 80 eV is given by

$$\sigma_{ab}(\Sigma S, E) = \sigma_{ab}(\Sigma S, 80) \left\{ \frac{\sigma_{rel}(\Sigma S, E)}{\sigma_{rel}(\Sigma S, 80)} \right\} \quad (21)$$

and

$$\sigma_{rel}(\Sigma S, E) = \sum_S \left(\frac{f(S) \{ \sigma(S, E) / \sigma(S, 1000) \}}{\sum_S f(S)} \right) \quad (22)$$

where $f(S)$ is the weighting factor for state S , $\sigma(S, E)$, the cross section for state S at energy E and the subscripts denote relative (rel) or absolute (ab) values. Values of the ratio $\sigma(S, E)/\sigma(S, 1000)$ determined from theoretical curves are given in Table 13. The theoretical curves were available [CL-72] for the $b^1\Pi_u$, $b'^1\Sigma_u^+$, and $c_n'^1\Sigma_u^+$ states and the curve shapes for the $c_n^1\Pi_u$ and $o_n^1\Pi_u$ were assumed to be the same as for $c_n'^1\Sigma_u^+$; thus the states $c_n'^1\Sigma_u^+$, $c_n^1\Pi_u$, and $o_n^1\Pi_u$ were treated together. The oscillator strengths given in Table 13 are based on optical measurements [Ca-72, LM-68a] and high-energy electron loss spectra [GS-69d]. The use of these data as relative measures of the electron excitation cross-sections at energies as low as 1000 eV can be partially justified on the basis of the comparison of the relative intensities in electron loss spectra at high and low energy. Thus from the high- (33 keV)[GS-65] and low-energy (200 eV) [LS-66b] electron loss data, the ratios of intensities of comparable peaks (i. e., for excitation to a specific vibronic level) are essentially constant for the $b'^1\Sigma_u^+$, $b^1\Pi_u$, and $c^1\Pi_u$ states (although there are few data in the latter case); for the

Table 13. Relative Values of Cross Sections for the $b' 1\Sigma_u^+$, $b 1\Pi_u$, $c'_n 1\Sigma_u^+$, $c_n 1\Pi_u$, and $o_n 1\Pi_u$ States at High Energies and the Corresponding Oscillator Strengths

A. Relative Cross-Sections

$E(\text{eV})$	$\frac{\sigma(b, E)}{\sigma(b, 1000)}$	$\frac{\sigma(b, E)}{\sigma(b, 1000)}$	$\frac{\sigma(c', c, o; E)}{\sigma(c', c, o; 1000)}$	$\sigma_{\text{rel}}(\Sigma S, E)$
1000	1.00	1.00	1.00	1.00
600	1.49	1.48	1.43	1.45
300	2.55	2.46	2.21	2.34
100	5.09	5.22	3.63	4.31
80	5.74	5.83	3.79	4.69

B. Oscillator Strengths

State	f	State	f
$b' 1\Sigma_u^+$	0.24	$c_3 1\Pi_u$	0.22
$b 1\Pi_u$	0.20	$c_4 1\Pi_u$	0.0057
$c'_3 1\Sigma_u^+$	0.11	$c_n 1\Pi_u$	*
$c'_4 1\Sigma_u^+$	0.0175	$o_3 1\Pi_u$	0.075
$c'_n 1\Sigma_u^+$	*	$o_4 1\Pi_u$	0.031

* $n \geq 5$ and $c'_n 1\Sigma_u^+ + c_n 1\Pi_u$ have the f value 0.070.

$c'1\Sigma_u^+$ state, the ratios vary by about 30%. No data are available for the $o_n1\Pi_u$ states.

The results of applying Eqs. (21) and (22) as described above are shown in Table 14.

4.2.2 Cross-Section Values for Specific States

To obtain cross-section data for electron excitation to individual states for energies greater than 110 eV, the following relation was used:

$$\sigma_{ab}(S, E) = \sigma_{ab}(\Sigma S, 1000) \left(\frac{f(S) \{ \sigma(S, E) / \sigma(S, 1000) \}}{\sum_S f(S)} \right) \quad (23)$$

This relation is consistent with Eqs. (21) and (22). The values of the cross sections so obtained are listed in Table 15.

The cross-section data for electron excitation to individual states for energies between 110 and 23 eV were obtained as follows. The cross-section profile for the $c'1\Sigma_u^+$ state is known to low energies; the theoretical curve [CL-72] and experimental curve shapes [AD-71] agree very well. By using this profile and the absolute value at 110 eV, as determined with Eq. (23), the absolute values of the cross section for the combination of the $c_n'1\Sigma_u^+$, $c_n1\Pi_u$, and $o_n1\Pi_u$ states were calculated from the relation

$$\sigma_{ab}(S, E) = 0.571 \sigma_{rel}(S, E) / \sigma_{rel}(S, 110) \quad (24)$$

where 0.571 is the absolute cross-section in units of 10^{-16} cm^2 for excitation to the above combination of states as determined from Eq. (23) and the ratio of cross sections in Eq. (24) was found from the c' state

Table 14. Absolute Cross-Sections for the a $^1\Pi_g$ and Predissociating States.

Energy (eV)	$\sigma(a^1\Pi_g)^*$	$\sigma(\text{pre})^\dagger$	Energy (eV)	$\sigma(a^1\Pi_g)$	$\sigma(\text{pre})$
11	0.077	-	110	0.070	1.23
14	0.292	0.0147	140	0.056	1.10
18	0.321	0.093	180	0.045	0.95
23	0.293	0.32	230	0.036	0.82
29	0.231	0.508	290	0.029	0.71
36	0.190	0.78	360	0.024	0.61
45	0.156	1.09	450	0.020	0.53
57	0.126	1.28	570	0.016	0.45
72	0.102	1.43	720	0.013	0.38
90	0.083	1.34	900	0.010	0.32

* Cross-sections in units of 10^{-16} cm^2 .

† Pre represents the states $b'^1\Sigma_u^+$, $b^1\Pi_u$, $c_n'^1\Sigma_u^+$, $c_n^1\Pi_u$, and $o_n^1\Pi_u$.

Table 15. Absolute Cross-Sections for the States $c'_n 1\Sigma_u^+$, $c_n 1\Pi_u$, $o_n 1\Pi_u$, $b' 1\Sigma_u^+$, and $b 1\Pi_u$.

<u>E (eV)</u>	<u>$\sigma(c', c, o)^*$</u>	<u>$\sigma(b')^\dagger$</u>	<u>$\sigma(b)^\ddagger$</u>
14	0.013	0.001	0.0007
18	0.084	0.005	0.004
23	0.288	0.017	0.015
29	0.429	0.043	0.036
36	0.532	0.135	0.113
45	0.592	0.271	0.227
57	0.618	0.361	0.301
72	0.618	0.442	0.370
90	0.601	0.403	0.336
110	0.571	0.359	0.300
140	0.526	0.313	0.261
180	0.468	0.264	0.218
230	0.412	0.220	0.180
290	0.361	0.190	0.159
360	0.321	0.163	0.136
450	0.278	0.137	0.115
570	0.239	0.115	0.096
720	0.205	0.095	0.080
900	0.174	0.079	0.067

* Cross-sections are in units of 10^{-16} cm^{-2} ; c' , c , o represents the combination of $c'_n 1\Sigma_u^+$, $c_n 1\Pi_u$, and $o_n 1\Pi_u$ states.

† b' represents $b' 1\Sigma_u^+$.

‡ b represents $b 1\Pi_u$.

profile. Absolute cross-sections for excitation to the $b' \ ^1\Sigma_u^+$ and $b \ ^1\Pi_u$ states were found by difference, i. e. ,

$$\sigma_{ab}(\Sigma S, E) - \sigma_{ab}(c', c, o; E) = \sigma(b', E) + \sigma(b, E) \quad (25)$$

with the further assumption that

$$\sigma(b, E)/\sigma(b'/E) = \sigma(b, 110)/\sigma(b'/110) \quad . \quad (26)$$

Below 23 eV, the relative values of all cross sections were kept constant. The entire set of cross-section values is presented in Table 15. The data of Table 15 are relevant to the choice of fractional predissociations presented in Table 12. For the $b \ ^1\Pi_u$ state, the maximum branching ratio is 0.31. Thus the uncertainty in this case is 0.24 of the total cross-section and repeat calculations were performed to avoid introducing this uncertainty.

4.3 CONSISTENCY AND COMPARISON OF RESULTS

A comparison of the predicted value of electron volts per ion pair based on the cross-section values established in Section 4.2 with the observed value for N_2 is a reasonable test of the validity of these cross sections. The cross sections for excitation to the predissociating states of N_2 account for at least 60% of the total cross-section for excitation of N_2 above 30 eV, 80% above 45 eV, and 85% above 140 eV according to the accounting employed in this report.

The predicted value of the electron volts per ion pair for N_2 is 35.87 at 900 eV and becomes 35.36 eV at 20,000 eV. The extension of the calculation from 900 to 20,000 eV reduces the electron volts per ion pair by an amount which is insensitive to the absolute cross-section values as compared between the present

calculations and others [TA-74a; SK-75]. The measured value of electron volts per ion pair at 20,000 eV is determined [IG-67] to be 34.8 ± 0.2 (a previous assessment [Wh-63b] yields 34.6 ± 0.3). Thus the predicted value is about 0.6 eV larger than the observed value. This, however, is not a significant difference as it corresponds only to a 9% error in the total cross-sections and this is less than any experimental error in measuring cross-sections. Therefore, the set of cross-sections for electron excitation to the $b\ ^1\Pi_u$, $b'\ ^1\Sigma_u^+$, $c_n\ ^1\Pi_u$, $c'_n\ ^1\Sigma_u^+$, $o_n\ ^1\Pi_u$, and $a''\ ^1\Sigma_g^+$ states of N_2 is consistent with observations on electron- N_2 interactions as measured by the value of the electron volts per ion pair.

An alternate set of cross sections [Wi-66] is frequently used [OJ-75] for calculating the formation of nitrogen atoms as a result of predissociation and dissociative ionization. When account is taken of the contribution of dissociative excitation, and ionization to this set and the total excitation cross-section curve derived from Winter's data based on the fractional predissociations given in Table 12, the calculated value of electron volts per ion pair in N_2 becomes 40.78 at 900 eV and 40.26 at 20,000 eV. These values are substantially larger than the observed best value of 34.8 and indicate that the cross sections derived from Winter's experiments [Wi-66] are too large. Note should be taken that the experimental technique used [Wi-66] is subject to large errors and that the experimental results have not been checked by other investigators.

5. REFERENCES

- AD-71 J. F. M. Aarts and F. J. DeHeer, Emission Cross Sections for NI and NII Multiplets and Some Molecular Bands for Electron Impact on N₂, Physica 52, 45 (1971).
- An-71c R. Anderson, A Compilation of Measured Lifetimes of Gaseous Diatomic Molecules, Atomic Data 3, 227 (1971).
- BC-66 A. J. Blake, J. H. Carver and G. N. Haddad, Photo-Absorption Cross Sections of Molecular Oxygen Between 1250 Å and 2350 Å, J. Quant. Spectry. Rad. Transfer 6, 451 (1966).
- BC-67 A. J. Blake and J. H. Carver, Determination of Partial Photoionization Cross Sections by Photoelectron Spectroscopy, J. Chem. Phys. 47, 1038 (1967).
- BC-69 J. Berkowitz and W. A. Chupka, Photoelectron Spectroscopy of Autoionized Peaks, J. Chem. Phys. 51, 2341 (1969).
- Be-30 H. Bethe, Zur Theorie des Durchgangs schneller Korpuskularstrahlen durch Materie, Ann. Physik 5, 325 (1930).
- Bo-72 W. L. Borst, Excitation of Several Important Metastable States of N₂ by Electron Impact, Phys. Rev. A5, 648 (1972).
- BS-69 D. J. Burns, F. R. Simpson and J. W. McConkey, Absolute Cross Sections for Electron Excitation of the Second Positive Bands of Nitrogen, J. Phys. B (Atom. Molec. Phys.) 2, 52 (1969).
- BT-70b R. T. Brinkmann and S. Trajmar, Electron Impact Excitation of N₂, Ann. Geophys. 26, 201 (1970).
- BW-69 K. D. Beyer and K. H. Welge, Photodissociation of O₂ and N₂ in the Far Vacuum UV and Production of Excited O and N Atoms, J. Chem. Phys. 51, 5323 (1969).
- Ca-72 V. L. Carter, High Resolution N₂ Absorption Study from 730 to 980 Å, J. Chem. Phys. 56, 4195 (1972).

- CC-65 G. R. Cook and B. K. Ching, Absorption, Photoionization, and Fluorescence of Some Gases of Importance in the Study of the Upper Atmosphere, SSD-TDR-64-16, 30 Jan. 1965.
- CC-69 P. K. Carroll and C. P. Collins, High Resolution Absorption Studies of the $b^1\pi_u \leftarrow X^1\Sigma_g^+$ System of Nitrogen, Can. J. Phys. 47, 563 (1969).
- CC-70b P. K. Carroll, C. P. Collins and K. Yoshino, The High Energy $1^1\Sigma_u^+$ States of N_2 , J. Phys. B 3, L127 (1970).
- CI-72 CIRA-1972, COSPAR International Reference Atmosphere, 1972, Compiled by COSPAR Working Group A, Akademie-Verlag, Berlin, 1972.
- CJ-71a R. W. Carlson and D. L. Judge, Photoionization Excitation of the $A^2\Pi_u$ State of O_2^+ , J. Chem. Phys. 54, 1832 (1971).
- CL-72 S. Chung and C. C. Lin, Excitation of the Electronic States of the Nitrogen Molecule by Electron Impact, Phys. Rev. A6, 988 (1972).
- CM-72c G. R. Cook and R. J. McNeal, Photoionization of Vibrationally Excited Nitrogen, J. Chem. Phys. 56, 1388 (1972).
- CO-65 G. R. Cook and M. Ogawa, Photoionization of N_2 in the 734 - 805 Å Region, Can. J. Phys. 43, 256 (1965).
- CS-65a R. B. Cairns and J. A. R. Samson, Total Absorption Cross Section of Atomic Oxygen Below 910 Å, Phys. Rev. 139 A1403 (1965).
- CS-68a F. J. Comes, F. Speier and A. Elzer, Photoionization Study of Atomic Beams. II. The Ionization Cross Section of Atomic-Oxygen, Z. Naturforsch 23a, 125 (1968). (In German).
- CY-72a P. K. Carroll and K. Yoshino, The $c_n^1\pi_u$ and $c_n^1\Sigma_u^+$ Rydberg States of N_2 : High Resolution Studies, J. Phys. B 5, 1614 (1972).

- DL-71 A. Dalgarno and G. Lejeune, The Absorption of Electrons in Atomic Oxygen, Planet. Space Sci. 19, 1653 (1971).
- Dr-69 K. Dressler, The Lowest Valence and Rydberg States in the Dipole-Allowed Absorption Spectrum of Nitrogen. A Survey of Their Interactions, Can. J. Phys. 47, 547 (1969).
- FW-69 S. V. Filseth and K. H. Welge, Production of O(¹S) in the Photodissociation $O_2 \rightarrow O(^1S) + O(^3P)$, J. Chem. Phys. 51, 839 (1969).
- GS-65 J. Geiger and W. Stickel, Energy Losses of Fast Electrons in Nitrogen, J. Chem. Phys. 43, 4535 (1965).
- GS-69d J. Geiger and B. Schröder, Intensity Perturbations Due to Configuration Interaction Observed in the Electron Energy-Loss Spectrum of N₂, J. Chem. Phys. 50, 7 (1969).
- HC-69 R. D. Hudson and V. L. Carter, Atmospheric Implications of Predissociation in N₂, J. Geophys. Res. 74, 393 (1969).
- He-50 G. Herzberg, Molecular Spectra and Molecular Structure. I. Spectra of Diatomic Molecules, Second Edition, D. Van Nostrand Co., Inc., Princeton, N. J., 1950.
- He-67b R. J. W. Henry, Photoionization Cross Sections for Atomic Oxygen, Planet. Space Sci. 15, 1747 (1967).
- He-68a R. J. W. Henry, The Influence of Autoionizing States on Absorption Cross Sections for Atomic Oxygen, Planet. Space Sci. 16, 1503 (1968).
- Ho-69b R. F. Holland, Excitation of Nitrogen by Electrons: The Lyman-Birge-Hopfield System of N₂, J. Chem. Phys. 51, 3940 (1969).
- HS-75 D. A. Hamlin and M. R. Schoonover, Ambient Atmosphere (Major and Minor Neutral Species and Ionosphere) [Model I], Vol. 2A of Atmospheric, Geomagnetic, and High-Altitude Energy-Deposition and Neutral-Particle-Motion Models for ROSCOE, Science Applications, Inc. Report No. SAI-75-609-LJ-2A, 13 June 1975.

- HT-63 R. E. Huffman, Y. Tanaka and J. C. Larrabee, Absorption Coefficients of Nitrogen in the 1000 - 580 Å Wavelength Region, J. Chem. Phys. 39, 910 (1963).
- Hu-69 R. E. Huffmann, Absorption Cross Sections of Atmospheric Gases for Use in Aeronomy, Can. J. Chem. 47, 1823 (1969).
- Hu-72a R. E. Huffman, Photochemical Processes: Cross-Section Data, Ch. 12 in Defense Nuclear Agency Reaction Rate Handbook, Second Edition, Revision No. 1, DNA 1948H, M. H. Bortner and T. Baurer, Editors, November 1972.
- IG-67 B. M. Isaev, I. V. Gordeev, Yu. I. Bregadze, Yu. S. Gerasimov and G. N. Antipenkova, Ion-Formation Energy of Charged Particles in Gases, Izmeritel'naya Tekhnika (USSR), No. 4, pp. 3-13 (April 1967). Translation in Meas. Tech. (USA) No. 4, pp. 389-401 (April 1967).
- JW-68 D. L. Judge and G. L. Weissler, Fluorescence Spectra of the Excited Ion N_2^+ Resulting from Vacuum-Ultraviolet Photon Impact on N_2 , J. Chem. Phys. 48, 4590 (1968).
- La-69 E. N. Lassettre, Inelastic Scattering of High Energy Electrons by Atmospheric Gases, Can. J. Chem. 47, 1733 (1969).
- LD-72 M. Leoni and K. Dressler, Deperturbation of the Worley-Jenkins Rydberg Series of N_2 , Hel. Phys. Acta 45, 959 (1972).
- LM-68a G. M. Lawrence, D. L. Mickey and K. Dressler, Absolute Oscillator Strengths of the Strongest Bands with the Dipole-Allowed Absorption Spectrum of Nitrogen, J. Chem. Phys. 48, 1989 (1968).
- LS-66b E. N. Lassettre, A. Skerbile and V. D. Meyer, Quadrupole-Allowed Transitions in the Electron Impact Spectrum of N_2 , J. Chem. Phys. 45, 3214 (1966).
- MH-75a B. F. Myers, D. A. Hamlin and M. R. Schoonover, Calculated and Observed Photoelectron-Flux Spectra at Dawn, J. Atmos. Terr. Phys. 37, 387 (1975).

- MS-75 B. F. Myers and M. R. Schoonover, Electron Energy Degradation in the Atmosphere: Consequent Species and Energy Densities, Electron-Flux and Radiation Spectra, DNA 3513T (SAI-74-619-LJ), 3 January 1975 (U).
- MW-67 F. M. Matsunaga and K. Watanabe, Total and Photoionization Coefficients and Dissociation Continua of O₂ in the 580 - 1070 Å Region, Science of Light 16, 31 (1967).
- My-75 B. F. Myers, Midlatitude Density Profiles of Selected Atmospheric Species (Data Base for Minor Neutral Species in Model 1), Vol. 2B of Atmospheric, Geomagnetic, and High-Altitude Energy-Deposition and Neutral-Particle-Motion Models for ROSCOE, Science Applications, Inc. Report No. SAI-75-609-LJ-2B, 13 June 1975.
- OJ-75 E. S. Oran, P. S. Julienne and D. F. Strobel, The Aeronomy of Odd Nitrogen in the Thermosphere, J. Geophys. Res. 80, 3068-3076 (1975).
- SC-64 J. A. R. Samson and R. B. Cairns, Absorption and Photoionization Cross Sections of O₂ and N₂ at Intense Solar Emission Lines, J. Geophys. Res. 69, 4583 (1964).
- SH-66a J. O. Sullivan and A. C. Holland, A Congeries of Absorption Cross Sections for Wavelengths Less than 3000 Å, NASA CR-371, January 1966.
- SK-75 T. L. Stephens and A. L. Klein, Electron Energy Deposition in the Atmosphere, Vol. I, GE75TMP-7, General Electric TEMPO, Center for Advanced Studies, Santa Barbara, California, May 1975.
- SL-70a T. Shimazaki and A. R. Laird, A Model Calculation of the Diurnal Variation in Minor Neutral Constituents in the Mesosphere and Lower Thermosphere Including Transport Effects, J. Geophys. Res. 75, 3221 (1970).
- TA-74a P. W. Tarr, D. H. Archer and N. G. Utterback, Studies of Auroral Simulation, DNA 3297F, (MRC-R-122), 11 April 1974.

- TW-72 S. Trajmar, W. Williams and A. Kuppermann, Angular Dependence of Electron Impact Excitation Cross Sections of O₂, J. Chem. Phys. 56, 3759 (1972).
- Wa-58 K. Watanabe, Ultraviolet Absorption Processes in the Upper Atmosphere, Advances in Geophysics, Edited by H. E. Landsberg and J. Van Miegham, Academic Press, 1958, pp. 153-221.
- Wh-63b G. N. Whyte, Energy per Ion Pair for Charged Particles in Gases, Radiation Research 18, 265 (1963).
- Wi-66 H. F. Winters, Ionic Absorption and Dissociation Cross Section for Nitrogen, J. Chem. Phys. 44, 1472 (1966).
- WM-67 K. Watanabe, F. M. Matsunaga and H. Sakai, Absorption Coefficient and Photoionization Yield of NO in the Region 580-1350 Å, Applied Optics 6, 391 (1967).
- WS-66 W. L. Wiese, M. W. Smith and B. M. Glennon, Atomic Transition Probabilities. Vol. I. Hydrogen Through Neon, National Standard Reference Data Series, National Bureau of Standards, Number 4, 20 May 1966.
- WZ-53 K. Watanabe, M. Zelikoff and E. C. Y. Inn, Absorption Coefficients of Several Atmospheric Gases, AFCRC Technical Report 53-23, June 1953.
- YT-75 K. Yoshino, Y. Tanaka, P. K. Carroll and P. Mitchell, High Resolution Absorption Spectrum of N₂ in the Vacuum-uv Region, $\text{o}_{3,4} \text{ } ^1\Pi_u \leftarrow \text{X } ^1\Sigma_g^+$ Bands, J. Molec. Spectros. 54, 87 (1975).

APPENDIX A

GUIDE TO DATA AVAILABLE ON MICROFICHE

A.1 The following is a guide to the detailed results of the calculations in this report. These results have been recorded on microfiche and are available from the authors in this form. * The calculations have been made with two codes: ISRADU which was used for the UV photon deposition described in Section 2 above and ISRAD which was used for the electron deposition described in Section 3 above. The guide to the latter code results has already been given [MS-75] and only corrections in this case are given below.

A.2 The identification of the calculations with the numbers on the upper right hand and left hand corners of the microfiche is given in Table A1 for the ISRADU code and in Table A2 for the ISRAD code. For each microfiche number (M.N.) appearing in the upper left hand corner, there corresponds a series of numbers (SERIES) appearing in the upper right hand corner. In the case of the ISRADU code calculations, the information in Table A1a identifies the results that appear on each microfiche; the variation from one microfiche to another is the result only of the change in the photon group - this change is identified in Table A1b. Corrections to the microfiche listed in Table A1b are given in M. N. 676 and are described in paragraph 32 of Section A. 3 below. In the case of the ISRAD code calculations, the microfiche numbers and series numbers apply in the order indicated in Table A2; corrections to these microfiche are given in M. N. 633 and are described in paragraph 32 of Section A. 3 below.

* The 216 microfiche have not been distributed with this report owing to their large bulk.

Table A-1. Identification of Microfiche Data for ISRADU Calculations

A-1a. Common Information on Each Microfiche

[O], cm ⁻³	[N ₂], cm ⁻³	[O ₂], cm ⁻³	θ , eV	ALT, km	Series	ETHRM*
2.0 (10)	5.21(15)	1.40(15)	0.0215	60	001	1.0(1)
					001, 002	1.0(8)
					002	1.0(10)
					002, 003	1.0(12)
3.23(11)	1.58(12)	2.5 (11)	0.0221	110	003, 004	1.0(5)
					004	1.0(7)
					004, 005	1.0(9)
2.98(10)	3.78(10)	4.21(9)	0.0847	145	005	2.0(5)
					006	2.0(7)
					006, 007	2.0(9)
1.91(9)	4.35(8)	2.74(7)	0.1105	250	007	6.3(5)
					007, 008	6.3(7)
					008, 009	6.3(9)
2.5 (13)	1.0 (8)	1.0 (8)	0.218	500	009	2.6(5)
1.0 (10)	5.21(15)	1.0 (10)	0.0215	100	009, 010	1.0(5)
1.0 (10)	1.0 (10)	1.4 (15)	0.0215	100	010, 011	1.0(5)

A-1b. Microfiche Numbers for Photon Energies

I	ENGGRP [#]	M. N.	I	ENGGRP	M. N.
6	10.01	237	50	20.67	053
12	11.43	231	54	24.40	034
17	12.52	199	60	33.67	033
28	13.71	204	64	40.80	852
31	14.84	200	69	65.44	854
36	15.74	084	72	130.41	856
45	17.63	057	82	281.05	859

* ETHRM = background electron density, cm⁻³

ENGGRP = Energy of photon group, eV

+ I = photon group identification number on microfiche

Table A-2. Identification of Microfiche Data for ISRAD Calculations

[O], cm ⁻³	[N ₂], cm ⁻³	[O ₂], cm ⁻³	θ, eV	ETHRM [*]	ENGGRP ⁺	ALT, km	M. N.	Series
2.0 (10)	5.21(15)	1.40(15)	0.0215	1.0(1) 1.0(8) 1.0(10) 1.0(12)	900 to 14 incl.	60	185	001-004 004-008 001-004 004-008
3.23(11)	1.58(12)	2.50(11)	0.0221	1.0(5) 1.0(7) 1.0(9)		110	588	001-004 004-008 008-011
2.98(11)	3.78(10)	4.21(9)	0.0847	2.0(5) 2.0(7) 2.0(9)		145	661	001-004 004-008 008-011
1.91(9)	4.35(8)	2.74(7)	0.1656	6.3(5) 6.3(7) 6.3(9)		250	666	001-004 004-008 008-011
2.5(13)	1.0(8)	1.0(8)	0.218	2.6(5)		500	715	001-004
1.0(10)	5.21(15)	1.0(10)	0.0215	1.0(5)		100	715	004-008
1.0(10)	1.0(10)	1.4(15)	0.0215	1.0(5)		100	715	008-011

* ETHRM = background electron density, cm⁻³

+ ENGGRP = energy of photon group, eV

A.3 The microfiche for the ISRADU runs contain the following data:

1. The first data of interest are the five columns headed by symbols N , $U(N)$, $DEL\ U(N)$, $W(N)$, and empty heading. The N is the index for the energy bin and is equal to $j+1$ (see Table 1 of MS-75); $U(N)$, $DEL\ U(N)$, and $W(N)$ correspond to U_{j+1} , ΔU_{j+1} , and W_{j+1} of Table 1 (of MS-75). The column with no symbol heading is the electron speed, v_{j+1} , in cm sec^{-1} .
2. The section of print beginning TERMS IN E(U) EQU., PHOTOABSORPTION can be neglected. This is only used with a solar source for photons.
3. The next section of print, beginning TERMS IN E(U) EQU., EXCIT./DISSOC. NUMBER, gives values of the quantity $[e_k] v_k \sigma_{xd}(k, S) b_{xd}(k, j, S) [S]$ found in Equation (2). The order of presentation is: the first column gives W_j , the second entry k , the third entry S , the fourth entry the above product. If electrons from more than one energy group k excite or dissociate S , additional sets of three entries – k , S , product – are printed. Following the four slashes, the sum $\sum_k [e_k] v_k \sigma_{xd}(k, S) b_{xd}(k, j, S) [S]$ is given. The numbers 1, 13, and 14, representing S , correspond to ground electronic states of O, N_2 , and O_2 , respectively.
4. The section beginning TERMS IN E(U) EQU., EXCIT./DISSOC. (U = U PRIME) gives values of the quantity $v_j b_{xd}(j, j, S) \sigma_{xd}(j, S) [S]$ found in Equation (3) but is otherwise similar to the previous section.

5. The section beginning TERMS IN E(U) EQU., IONIZATION NUM. gives values of the quantity $[e_k] v_k \sigma_i(k, S) b_i(k, j, S)[S]$ found in Equation (2) but is otherwise identical to the section discussed in paragraph 3.
6. The section beginning TERMS IN E(U) EQU., IONIZATION (U = U PRIME) gives the values of the quantity $v_j b_i(j, j, S) \sigma_i(j, S)[S]$ found in Equation (3); otherwise paragraph 3 applies here.
7. The section beginning TERMS IN E(U) EQU., LOSS TO THERMAL ELEC. NUMER. lists values of k and $C_{j+1, j}[e_{j+1}]$, the latter being a term in Equation (2).
8. The section beginning TERMS IN E(U) EQU., EXCIT./DISSOC. DENOM. gives values of $v_j \sigma_{xd}(j, S)[S]$ as found in Equation (3). The first column gives U_j with further entries of S and $v_j \sigma_{xd}(j, S)[S]$.
9. The section beginning TERMS IN E(U) EQU., IONIZATION DENOM. gives values of $v_j \sigma_i(j, S)[S]$ but is otherwise similar to the previous section.
10. The section beginning TERMS IN E(U) EQU., LOSS TO THERMAL ELEC. DENOM. lists values of k and $C_{j, j-1}$; see Equation (3).
11. The next section gives a summary of the preceding sections. The headings and their reference are: ENERGY, the values of U_j ; S , the targets as listed; PA, not applicable here; XD and I, individual entries are $\sum_k e_k v_k \sigma_\alpha(k, S) b_\alpha(k, j, S)[S]$ for $\alpha = xd, i$ and sums are given below the dotted lines; TH gives $C_{j+1, j}[e_{j+1}]$; SIG+, the sum of XD, I, and TH; XD and I (the headings on the right-hand side of the table), individual entries are $\sum_k v_k \sigma_\alpha(k, S) b_\alpha(k, j, S)[S]$ for

$\alpha = xd$, i and sums are given as before; TH (heading on right-hand side of the page) gives $C_{j, j-1}$ and SIG-, the sum of XD, I, TH. The number above SIG- which is preceded by (is $[e_j]$ which is calculated from the ratio SIG+/SIG-.

12. The section beginning EXCIT./DISSOC. TERMS IN EQUATION 6A gives the quantities $[e_j] v_j \sigma_\alpha(j, S)$ for $\alpha = xd$ as found in Equation (4) of the text. The first entry is $N(=j+1)$, second entry is S , the third entry is an index redundant for reading the microfiche, and the fourth entry is the quantity given above.
13. The section beginning IONIZATION TERMS IN EQUATION 6A is identical to the previous section except that $\alpha = i$.
14. The section beginning EXCIT./DISSOC. TERMS IN EQUATION 6B gives the quantity $[e_j] v_j \sigma_\alpha(j, S) b_\alpha(j, S, S')[S]$ for $\alpha = xd$ which is found in Equation (5). The first four entries are N , S , S' , and the previous quantity. When $S = 1$, $S' = 1, 2, 3$, or 4 , and these numbers represent the products $O(^1D)$, $O(^1S)$, $O(3s^3S^\circ)$, and $O(3p^3P)$, respectively; when $S = 13$, $S' = 1, 2, 3, 4, 5, 6, 7, 8$, and these numbers represent the products

$$\left[N_2(A^3\Sigma_u^+), N_2(B^3\Pi_g), N_2(W^3\Delta_u), N_2(C^3\Pi_g) \right], N_2\left(c_n'^1\Sigma_u^+, c_n^1\Pi_u, \right. \\ \left. o_n^1\Pi_u \right), N_2(a''^1\Sigma_g^+), N_2(b'^1\Sigma_u^+), N_2(b^1\Pi_g), \left[N(^4S^\circ), N(^2D^\circ), N(^2P^\circ) \right]$$
 from decay of excited atoms formed in dissociative excitation, $N_2(X^1\Sigma_g^+)$ vibrationally excited; when $S = 14$, $S' = 1, 2, 3, 4, 5, 6, 7$, and these numbers represent the products

$$O_2(a^1\Delta_g), O_2(b^1\Sigma_g^+), O_2(c^1\Sigma_g^-), O_2(B^3\Sigma_u^-), \left[O(^3P), O(3s^3S^\circ) \right], \\ \left[O(^3P), O(3s^5S^\circ) \right], O_2(X^3\Sigma_g^-) \text{ vibrationally excited.}$$

15. The section beginning IONIZATION TERMS IN EQUATION 6B gives the quantity $[e_j]v_j \sigma_\alpha(j, S) b_\alpha(j, S, S')[S]$ for $\alpha = i$; see Equation (5). The listings are similar to those of the previous section but when $S = 1$, $S' = 1, 2, 3$, and these numbers correspond to the products $O^+(^4S^\circ)$, $O^+(^2D^\circ)$, $O^+(^2P^\circ)$, respectively; when $S = 13$, $S' = 1, 2, 3, 4$, and these numbers correspond to the products $N_2^+(A^2\Pi_u)$, $N_2^+(B^2\Sigma_u^+)$, $N_2^+(X^2\Sigma_g^+)$, and $[N^+(^3P) \text{ and } N(^4S^\circ)]$; when $S = 14$, $S' = 1, 2, 3, 4, 5$, and these numbers correspond to the products $O_2^+(X^2\Pi_g)$, $O_2^+(a^4\Pi_u)$, $O_2^+(A^2\Pi_u)$, $O_2^+(b^4\Sigma_g^-)$, and $[O^+(^4S^\circ) \text{ and } O(^3P)]$.
16. The section beginning PHOTOABSORPTION TERMS IN EQUATION 6B gives the quantity $\varphi(i) \sigma(i, S) b(i, S, S')[S]$ found in Eq. (5). When $S = 1$, $S' = 1, 2, 3$, and these numbers correspond to the products $O^+(^4S^\circ)$, $O^+(^2D^\circ)$, $O^+(^2P^\circ)$, respectively; when $S = 13$, $S' = 1, 2, 3, 4$, and these numbers correspond to the products $N(^4S^\circ)$, $N(^2D^\circ)$, $N_2^+(X^2\Sigma_g^+)$ and $N_2^+(A^3\Sigma_u^+)$ respectively; when $S = 14$, $S' = 1, 2, 3, 4, 5$, and these numbers correspond to the products $O(^3P)$, $O(^1D)$, $O(^1S)$, $O_2^+(X^2\Pi_g)$, and $O_2^+(a^4\Pi_u)$ respectively; when $S = 23$, $S' = 1, 2, 3, 4, 5, 6$, and these numbers correspond to the products $O(^3P)$, $O(^1S)$, $N(^4S^\circ)$, $N(^2D^\circ)$, $N(^2P^\circ)$, $NO^+(X^1\Sigma^+)$, respectively.
17. The section beginning EXCIT./DISSOC. TERMS IN KDOT EQU. lists the quantity $[e_j]v_j \epsilon_{M\alpha}(j, S) \sigma_\alpha(j, S)[S]$ as found in Equation (8) with $\alpha = xd$ and $M = K$. The four repeated entries are N, S, I, and the quantity given here.

18. The section beginning IONIZATION TERMS IN KDOT EQU. is the same as the previous section but with $\alpha = i$.
19. Paragraph 17 or 18 applies to the sections beginning EXCIT. / DISSOC. TERMS IN EDOT EQU., IONIZATION TERMS IN EDOT EQU., EXCIT. / DISSOC. TERMS IN RDOT EQU., IONIZATION TERMS IN RDOT EQU., and EXCIT. / DISSOC. TERMS IN XVDOT EQU. but with the set of values (α, M) equal to (xd, E) , (i, E) , (xd, R) , (i, R) , and (xd, X_v) , respectively.
20. The next data are printed in the form of four tables, which in view of the above guide, the text and reference MS-75, are readily understood. These tables list formation rates for the various species resulting from photoabsorption, excitation and ionization which are calculated according to Eq. (5). Radiation rates and fluorescent efficiencies are also listed; these are calculated as described in MS-75. The first two tables concern oxygen species. The first table gives uniquely the particles formed per ion pair; the second table, the particles formed per absorbed photon; otherwise the two tables are identical. The third and fourth tables concern nitrogen species and are distinguished as the first two tables are. The calculation of the radiation rates and florescent efficiencies are described in MS-75.
21. The next two tables are reductions of the preceding four tables. The reductions are made by taking into account the result of radiative transitions and dissociations (including predissociations). The radiative transitions taken into account are given in Table 4 of reference MS-75 (p. 28) and Table 3 of this report (p. 24). The dissociation or predissociation of molecules

(of the preceding four tables) [and products] are
 $O_2(B^3\Sigma_u^-)[O(^3P) + O(^1D)]$, $O_2(c^1\Sigma_u^-)[O(^3P) + O(^3P)]$,
 $N_2b^1\Pi_u[0.83N(^4S^\circ) + 0.83N(^2D^\circ)]$, $N_2(c_n'^1\Sigma_u^+, c_n^1\Pi_u, o_n^1\Pi_u)$
 $[0.125N(^4S^\circ) + 0.375N(^2D^\circ)]$, $N_2(b'^1\Sigma_u^+)[0.144N(^4S^\circ) +$
 $0.216N(^2D^\circ) \text{ or } 0.752N(^4S^\circ) + 1.128N(^4S^\circ)]$, $N_2(a''^1\Sigma_g^+)$
 $[N(^4S^\circ) + N_2(^2D^\circ)]$. For the alternate product sets in the

case of predissociation of $N_2(b'^1\Sigma_u^+)$, there are two sets of data given in these two tables. The corresponding energy transformation for all processes in the reduction are taken into account. Each table contains the formation rates for both oxygen and nitrogen species and the two tables differ by the inclusion of the quantity particles per ion pair formed in one and particles per absorbed photon in the other.

22. The line of print beginning VIBENG gives dX_v/dt for the four species indicated.
23. The next four lines show species densities for ground state O, N_2 , and O_2 ; the number on the first of the four lines is the O density and the first and second numbers of the second line are the N_2 and O_2 densities, respectively. The remaining numbers can be neglected.
24. The lines labeled PHI(I, T) give the photon flux (photons/cm²sec) where I indicates the position of the entry in the array and the photon energy corresponding to the value of I is given in Table A-1b.

AD-A043 324

SCIENCE APPLICATIONS INC LA JOLLA CALIF
UV PHOTON AND ELECTRON DEPOSITION IN THE ATMOSPHERE.(U)
AUG 76 B F MYERS, M R SCHOONOVER

F/G 20/8

UNCLASSIFIED

SAI-76-696-LJ

DNA-4068F

DNA001-74-C-0149

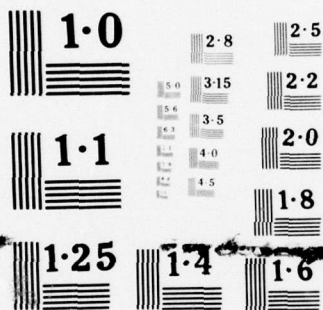
NL

2 OF 2
ADA
043324



END
DATE
FILMED

9-77
DDC



NATIONAL BUREAU OF STANDARDS
MICROCOPY RESOLUTION TEST CHART

25. The line beginning BIGI is not of interest in relation to the present calculations.
26. On the next line, beginning with THETA, the relevant items are THETA, the electron temperature, TEMP, the neutral particle temperature, THVIB, the vibrational temperature and YPCS, the altitude.
27. The next two lines contain in order, ETHRM, the electron density of electrons in the thermal group, $[e_{th}]$; SMEU, the electron density of electrons in the high energy groups, $\sum_j [e_j]$; SMUEU, the energy of the high-energy electrons, $\sum_j U_j [e_j]$; DETHDT, the rate of formation of thermal electrons, $d[e_{th}]/dt$; SEUETH, the ratio of the densities of high-energy to thermal electrons, $\sum_j [e_j]/[e_{th}]$; DOTUTA, the sum of the energy densities in the seven energy modes; SUMON5, the number of absorbed photons given by the denominator of Eq. (13).
28. In the next two lines, beginning with NGRP, the number of the photon group in which the photon belongs, the following quantities are listed: DELDT, the denominator of Equation (10); EVPIP, the electron volts per ion pair, E_{ip} of Equation (11), ENGGRP, the energy of the photon; SUMEDT, the sum of the rates of change of energy density in the seven energy modes; TERMON, the quantity $\sum_j [e_j] v_j \sigma_A(j, O_2)[O_2]$; SOKDOT, SODDOT, and SOIDOT, are not applicable to the present calculations.
29. The next two lines list, in order, the rates of change of energy density and the fractional contributions of the seven energy

modes, K, E, R, X_v , I, D, X_e (see Section 2.1.2) corresponding to the tables of paragraph 20.

30. The next four lines are the same as the corresponding four previous lines but apply to the tables of reduced data (see paragraph 21 above).
31. The seven columns with the headings N, U(N), E(TH)/DEL U, (E(TH) + E(N))/DEL U, F(N) PRIME, H(N) PRIME and E(N) represent: the energy-group index, $j+1$ (see Table 1 of MS-75); the energy group, U_{j+1} ; the differential thermal electron density contribution to each energy group; the differential total electron density contribution to each energy group, $[e_{\text{total}}]/\Delta U$; the total electron flux, ψ_{j+1} (see Equation (20)); the photoelectron flux; the electron density, $[e_{j+1}]$.
32. Because of a round-off error in calculating the thermal electron density, some of the columns headed E(TH)/DEL U, (E(TH) + E(N))/DEL U and F(N) PRIME may be in error. To correct these data by repeating the calculations is too expensive; rather, only the calculations for the thermal electron density and fluxes were repeated. These corrections are on microfiche no. (M.N.) 676 with the following format: the first two lines contain O, N_2 , O_2 , THETA, ETHRM, ALT where O, N_2 , and O_2 are followed by the respective densities, THETA by the electron temperature, ETHRM by the electron density, ALT by the altitudes for the calculations to which the corrections apply. The latter are identified in the third line and referenced table. Following these quantities, a table with the headings N, U(N), E(TH)/DEL and K(N) PRIME appears.

The first three quantities are defined in paragraph 31 above and $K(N)$ PRIME is the thermal electron flux. The corrected value of the total electron flux is obtained from the relation $F(N)$ PRIME = $K(N)$ PRIME + $H(N)$ PRIME, the latter quantity being obtained as indicated in paragraph 31.

33. The final group of data labeled $U(J), S, S(\text{SIGMA})$, and repeats, gives the energy group (see Table 1 of MS-75), the target, and the loss function (Equation 26 of MS-75). The last column, column 10, gives values of $[e_j] v_j \sigma_A(j, O_2) [O_2]$
- A. 4 The guide to the microfiche for ISRAD calculations has been previously presented (MS-75); here, only the changes are given for the items of MS-75.
14. The quantity $[e_j] v_j \sigma_\alpha(j, S) [S]$ is incorrect; the correct quantity is $[e_j] v_j \sigma_\alpha(j, S)$.
16. Replace $N_2(c \ 1_\Sigma^+)$ by $N_2(c'_n \ 1_\Sigma^+, c_n \ 1_\Pi_u, o_n \ 1_\Pi_u)$.
28. Replace EUPIP by EVPIP; replace TERMUM by TERMOM.
31. The corrections discussed in paragraph 32 of Section A. 3 apply here with the following changes: the corrections are on microfiche no. (M. N.) 633; the calculations to which the corrections apply are identified on the third line.

DISTRIBUTION LIST

DEPARTMENT OF DEFENSE

Director
Defense Advanced Research Proj. Agency
ATTN: Strategic Tech. Office

Defense Documentation Center
12 cy ATTN: TC

Director
Defense Nuclear Agency
ATTN: STSI, Archives
ATTN: DDST
3 cy ATTN: STIL, Tech. Library
ATTN: RAAE

Dir. of Defense Research & Engineering
Department of Defense
ATTN: S&SS (OS)

Commander
Field Command
Defense
ATTN: FCPR

Director
Interservice Nuclear Weapons School
ATTN: Document Control

Chief
Livermore Division, Field Command, DNA
Lawrence Livermore Laboratory
ATTN: FCPRL

DEPARTMENT OF THE ARMY

Commander
Harry Diamond Laboratories
2 cy ATTN: DRXDO-NP

Director
TRASANA
ATTN: ATAA-SA

Director
US Army Ballistic Research Labs.
ATTN: Tech. Lib.
ATTN: Mark D. Kregel
ATTN: DRXBR-AM, D. Snider
ATTN: I. L. Chidsey
ATTN: John C. Mester

Commander
US Army Electronics Command
ATTN: DRSEL-PL-ENV, Hans A. Bonke

Commander
US Army Foreign Science & Tech. Center
ATTN: R. Jones

Commander
US Army Nuclear Agency
ATTN: MONA-WE, J. Berberet

DEPARTMENT OF THE NAVY

Chief of Naval Research
Navy Department
ATTN: Code 461, R. Gracen Joiner

Commander
Naval Ocean Systems Center
ATTN: Code 2200, Jurgen Richter
ATTN: William F. Moler
ATTN: Technical Library
ATTN: Code 2200, Verne E. Hildebrand
ATTN: Code 2200, Ilan Rothmuller

Director
Naval Research Laboratory
ATTN: Code 7700, Timothy P. Coffey
ATTN: Code 7701, Jack D. Brown
ATTN: Code 2600, Tech. Lib.
ATTN: Code 7127, Charles Y. Johnson
ATTN: Code 7750, S. L. Ossakow
ATTN: Code 7750, Darrell F. Strobel
ATTN: Code 7750, Wahab Ali
ATTN: Code 7750, J. Davis

Commander
Naval Surface Weapons Center
ATTN: Code WA501, Navy Nuc. Prgms. Off.

DEPARTMENT OF THE AIR FORCE

AF Geophysics Laboratory, AFSC
ATTN: LKO, Robert E. Huffman
ATTN: LKB, William Swider, Jr.
ATTN: LKB, A. Faire
ATTN: LKB, Kenneth S. W. Champion
ATTN: OPR, James C. Ulwick
ATTN: LKB, Edmond Murad
ATTN: LKB, John Paulson
ATTN: LKB, T. J. Keneshea
ATTN: LKS, R. A. Van Tassel
ATTN: LKD, C. R. Philbrick
ATTN: LKD, Rocco S. Narcisi
ATTN: LKS, F. R. Innes
ATTN: OPR, Harold Gardner
ATTN: OPR, Alva T. Stair
ATTN: OPR, F. DelGreco
ATTN: OPR, R. E. Murphy
ATTN: OPR, J. Kennealy
ATTN: OPR, R. O'Neill
ATTN: SUOL, Research Library

AF Weapons Laboratory, AFSC
ATTN: SUL

Commander
Foreign Technology Division, AFSC
ATTN: NICD, Library

Commander
Rome Air Development Center, AFSC
ATTN: OCSE, J. J. Simons

ENERGY RESEARCH & DEVELOPMENT ADMINISTRATION

EG&G, Inc.
Los Alamos Division
ATTN: James R. Breedlove

University of California
Lawrence Livermore Laboratory
ATTN: A. Kaufman, L-96

Los Alamos Scientific Laboratory
ATTN: Doc. Con. for T. Bieniewski, CMB-1
ATTN: Doc. Con. for John Zinn
ATTN: Doc. Con. for R. A. Jeffries

OTHER GOVERNMENT AGENCIES

Department of Commerce
Office of Telecommunications
Institute for Telecom Science
ATTN: Glenn Falcon
ATTN: William F. Utlaut

National Bureau of Standards
ATTN: Stephen J. Smith, JILA
ATTN: Gordon H. Dunn, JILA
ATTN: A. V. Phelps, JILA
ATTN: Peter L. Bender, JILA

National Oceanic & Atmospheric Admin.
Environmental Research Laboratories
Department of Commerce
ATTN: Eldon Ferguson
ATTN: Fred Fehsenfeld

National Science Foundation
ATTN: Rolf Sinclair

DEPARTMENT OF DEFENSE CONTRACTORS

Aerodyne Research, Inc.
ATTN: M. Camac

Aeronomy Corporation
ATTN: S. A. Bowhill

AVCO-Everett Research Laboratory, Inc.
ATTN: C. W. Von Rosenberg, Jr.

University of Denver
Colorado Seminary
Denver Research Institute
ATTN: Sec. Officer for David Murcray

Epsilon Laboratories, Inc.
ATTN: Henry Miranda

General Electric Company
Space Division
Valley Forge Space Center
ATTN: M. H. Bortner, Space Sci. Lab.
ATTN: F. Alyea
ATTN: T. Baurer

DEPARTMENT OF DEFENSE CONTRACTORS (Continued)

General Electric Company
TEMPO-Center for Advanced Studies
ATTN: Tim Stephens
ATTN: Warren S. Knapp
ATTN: DASIAC
ATTN: J. Schoutens
ATTN: Mack Stanton
ATTN: James H. Thompson
ATTN: Don Chandler
ATTN: L. Ewing

HSS, Inc.
ATTN: Donald Hansen
ATTN: M. P. Shuler

Institute for Defense Analyses
ATTN: Hans Wolfhard
ATTN: Ernest Bauer

ION Physics Corporation
ATTN: Charles R. Hauer

IRT Corporation
ATTN: R. H. Neynaber

Lockheed Missiles & Space Company, Inc.
ATTN: John Kumer
ATTN: John L. Kulander, Dept. 52-14
ATTN: Martin Walt, Dept. 52-10
ATTN: Richard G. Johnson, Dept. 52-12

Mission Research Corporation
ATTN: D. Sappenfield
ATTN: P. Fischer
ATTN: M. Scheibe
ATTN: Dave Sowle

Photometrics, Inc.
ATTN: Irving L. Kofsky

Physical Dynamics, Inc.
ATTN: Joseph B. Workman

University of Pittsburgh of the Comwlth. Sys. of
Higher Education
Cathedral of Learning
ATTN: Wade L. Fite
ATTN: Manfred A. Biondi
ATTN: Frederick Kaufman

R & D Associates
ATTN: Forrest Gilmore
ATTN: Robert E. LeLevier
ATTN: R. P. Turco

Science Applications, Inc.
ATTN: Ben Myers
ATTN: Melvin R. Schoonover
ATTN: Daniel A. Hamlin

Stanford Research Institute
ATTN: Walter G. Chestnut
ATTN: D. J. Hildenbrand

Utah State University
ATTN: Kay Baker

VisiDyne, Inc.
ATTN: J. W. Carpenter
ATTN: Charles Humphrey